Article

Immunity

IL-1 Family Cytokines Use Distinct Molecular Mechanisms to Signal through Their Shared Co-receptor

Graphical Abstract

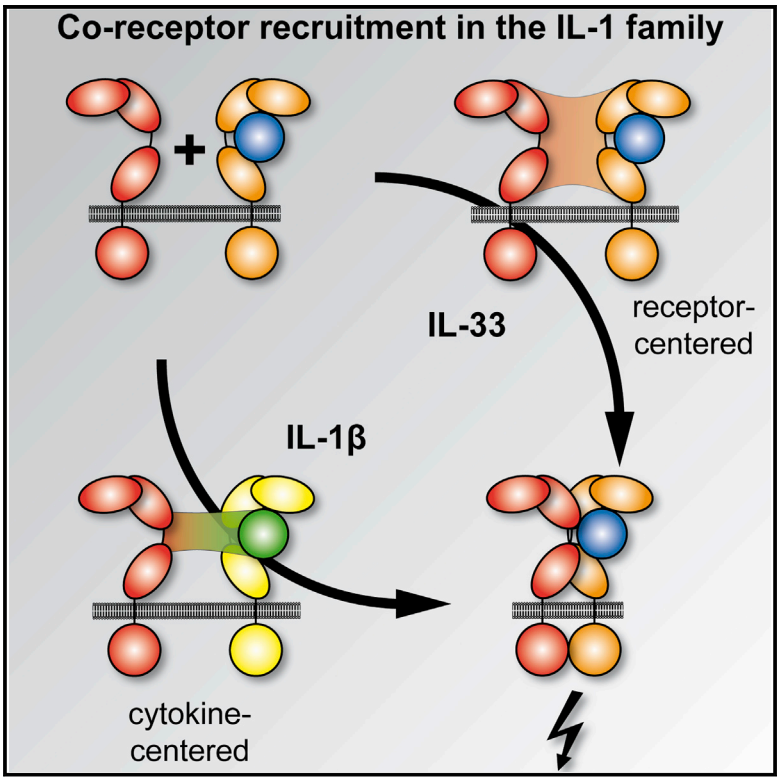

Highlights

- Generated 2.8 Å X-ray crystal structure of the IL-33-ST2-IL-1RAcP signaling complex
- IL-1RAcP uses the same motifs to engage different cytokine-receptors pairs
- IL-1β and IL-33 form signaling complexes by distinct molecular mechanisms

Authors

Sebastian Günther, Daniel Deredge, Amanda L. Bowers, ..., Lance Liotta, Patrick L. Wintrode, Eric J. Sundberg

Correspondence

esundberg@ihv.umaryland.edu

In Brief

IL-1RAcP is the co-receptor shared by most cytokines in the IL-1 family. Günther et al. demonstrate that although IL-1RAcP interacts with different cytokine-receptor pairs through a conserved architecture, it uses starkly different strategies to engage IL-1β and IL-33 and form signaling-competent ternary complexes.

Günther et al., 2017, Immunity *47*, 510–523
September 19, 2017
http://dx.doi.org/10.1016/j.immuni.2017.08.004

CellPress

Immunity
Article

IL-1 Family Cytokines Use Distinct Molecular Mechanisms to Signal through Their Shared Co-receptor

Sebastian Günther,[1] Daniel Deredge,[2] Amanda L. Bowers,[1] Alessandra Luchini,[3] Daniel A. Bonsor,[1] Robert Beadenkopf,[1] Lance Liotta,[3] Patrick L. Wintrode,[2] and Eric J. Sundberg[1,4,5,6,*]

[1]Institute of Human Virology, University of Maryland School of Medicine, Baltimore, MD 21201, USA
[2]Department of Pharmaceutical Sciences, University of Maryland School of Pharmacy, Baltimore, MD 21201, USA
[3]Center for Applied Proteomics and Molecular Medicine, George Mason University, Manassas, VA 20110, USA
[4]Department of Medicine, University of Maryland School of Medicine, Baltimore, MD 21201, USA
[5]Department of Microbiology & Immunology, University of Maryland School of Medicine, Baltimore, MD 21201, USA
[6]Lead Contact
*Correspondence: esundberg@ihv.umaryland.edu
http://dx.doi.org/10.1016/j.immuni.2017.08.004

SUMMARY

Within the interleukin 1 (IL-1) cytokine family, IL-1 receptor accessory protein (IL-1RAcP) is the co-receptor for eight receptor-cytokine pairs, including those involving cytokines IL-1β and IL-33. Unlike IL-1β, IL-33 does not have a signaling complex that includes both its cognate receptor, ST2, and the shared co-receptor IL-1RAcP, which we now present here. Although the IL-1β and IL-33 complexes shared structural features and engaged identical molecular surfaces of IL-1RAcP, these cytokines had starkly different strategies for co-receptor engagement and signal activation. Our data suggest that IL-1β binds to IL-1RI to properly present the cytokine to IL-1RAcP, whereas IL-33 binds to ST2 in order to conformationally constrain the cognate receptor in an IL-1RAcP-receptive state. These findings indicate that members of the IL-1 family of cytokines use distinct molecular mechanisms to signal through their shared co-receptor, and they provide the foundation from which to design new therapies to target IL-33 signaling.

INTRODUCTION

The interleukin-1 (IL-1) family comprises 11 cytokines that are central regulators of immunity and inflammation. Agonist cytokines of this family bind their cognate receptors (e.g., the IL-1 receptor I [IL-1RI, also known as IL-1R1] for the prototypical agonist cytokines IL-1α and IL-1β) and subsequently recruit a co-receptor, most commonly IL-1 receptor accessory protein (IL-1RAcP, also known as IL-1R3), to form ternary complexes. The structural basis of the formation of IL-1β signaling complexes has been well defined by numerous X-ray crystal structures of this ternary complex comprising a cytokine, cognate receptor, and co-receptor (Thomas et al., 2012; Wang et al., 2010). Cytoplasmic Toll/IL-1 receptor (TIR) domains attached to the cognate and co-receptors are brought into close proximity by these extracellular binding events, resulting in signal transduction. Because of the potency of the cellular responses of IL-1 cytokines, several layers of negative regulation exist to inhibit the effects of these responses, including (1) antagonist cytokines (e.g., IL-1 receptor antagonist [IL-1Ra]), which bind to cognate receptors but do not recruit co-receptors; and (2) decoy receptors (e.g., IL-1RII [IL-1R2] or soluble suppression of tumorgenicity ST2 [also known as sST2, IL-1R4, IL-1RL1, T1, or IL-33R]), which lack trans-membrane regions and/or cytoplasmic TIR domains.

IL-33 is an agonist cytokine that binds its cognate receptor, ST2, and recruits the same co-receptor, IL-1RAcP, as that recruited by IL-1β. The crystal structure of the binary IL-33-ST2 complex (but not the ternary IL-33-ST2-IL-1RAcP complex) has been reported (Liu et al., 2013). No antagonist IL-33 cytokine exists, and IL-33 signaling is instead negatively regulated primarily by sST2 (which acts as a decoy receptor; Hayakawa et al., 2007), as well as by IL-33 oxidation (Cohen et al., 2015) and cleavage by caspases (Cayrol and Girard, 2009; Lüthi et al., 2009). IL-33 also contains an N-terminal nuclear localization domain that typically retains the cytokine in the nucleus where it is bound to chromatin (Carriere et al., 2007); the deletion of this domain causes IL-33-specific systemic inflammation (Bessa et al., 2014). With no signal sequence for secretion, IL-33 is instead released from damaged or necrotic endothelial and epithelial cells and acts as an alarmin to alert the immune system to tissue damage (Cayrol and Girard, 2014). Inflammatory proteases from neutrophils and mast cells process full-length IL-33 into mature forms, equivalent in molecular weight to other mature IL-1 family cytokines, with increased receptor binding and signaling activity (Lefrançais et al., 2014; Lefrançais et al., 2012).

IL-33 is predominantly expressed by epithelial, endothelial, and fibroblast cells (Liew et al., 2016). Because ST2 is presented on the surfaces of many immune cells, IL-33 has pleiotropic effects in health and disease and has wide-ranging roles in tissue and metabolic homeostasis, infection, inflammation, cancer, and neurological disorders. Originally thought to activate only T helper 2 (Th2) and mast cells (Schmitz et al., 2005), IL-33 is now known to stimulate diverse activated ST2-expressing leukocytes such as Th1 cells, regulatory T (Treg) cells, group 2 innate lymphoid cells (ILC2s), $CD8^+$ T cells, and natural killer (NK) cells.

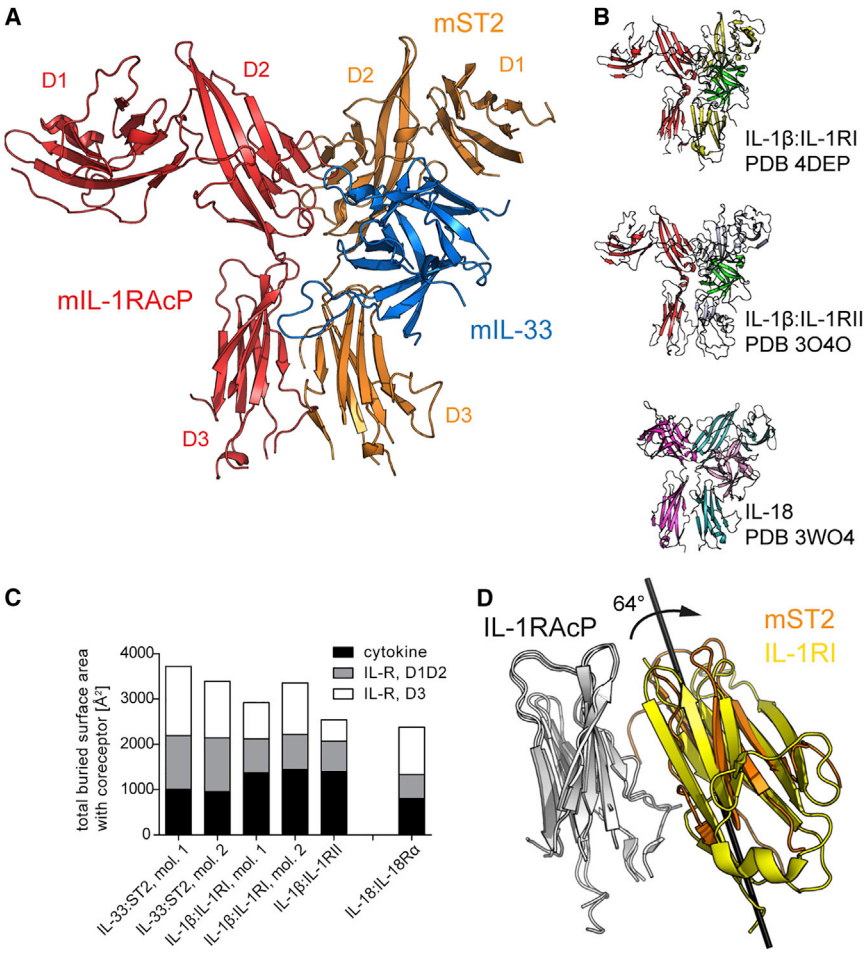

Figure 1. Crystal Structure of the IL-33 Signaling Complex

(A) Crystal structure of the murine IL-33:ST2:IL-1RAcP complex. Receptor subdomains are indicated.

(B) Crystal structure of other ternary complexes in the IL-1 family. Top: signaling complex of IL-1β:IL-1RI:IL-1RAcP. Middle: decoy complex of IL-1β:IL-1RII:IL-1RAcP. Bottom: signaling complex of IL-18:IL-18Rα:Il-18Rβ (same orientation as in A; the co-receptor is on the left, and the cytokine-primary-receptor is on the right).

(C) Comparison of buried surface areas at interfaces between binary cytokine-primary-receptor complexes and co-receptors as observed in crystal structures. IL-1RAcP-dependent complexes are shown on the left. Total areas are subdivided on the basis of cytokine and primary-receptor domains.

(D) Rotation of the ST2 D3 domain in relation to IL-1RI D3. IL1-RAcP D3 is shown in white. The rotation axis is indicated.

See also Figure S1.

IL-33 stimulation of Th2 cells, Treg cells, and ILC2s induces their proliferation, survival, and migration, as well as their production of the type 2 immune mediators IL-4, IL-5, and IL-13 (Lott et al., 2015; Molofsky et al., 2015). The type I immune mediator interferon-γ (IFN-γ) is produced by Th1 cells, $CD8^+$ T cells, and NK cells in response to IL-33 (Bonilla et al., 2012).

Collectively, these signaling events drive a vast network of immune and inflammatory processes. Although IL-33 is constitutively expressed at high levels, it can be further upregulated during inflammation. Accordingly, IL-33 signaling plays a central role in clearing infections by helminths, protozoa, fungi, bacteria, and viruses (Liew et al., 2016). As a potent mediator of inflammation, IL-33 can be responsible for a variety of chronic inflammatory disorders. IL-33 is deleterious in asthma, allergy, rheumatoid arthritis, inflammatory bowel disease, chronic obstructive pulmonary disease, age-related macular degeneration, and periodontitis. Conversely, IL-33 confers beneficial effects in cardiovascular diseases, obesity, diabetes, and uveitis (Liew et al., 2016).

Given the central involvement of IL-33 in these diseases, there is considerable interest in the development of biologics for modulating its activity. IL-1 signaling has already been successfully targeted in a number of auto-inflammatory conditions through the use of several biologics, including antagonist cytokines, decoy receptors, and antibodies (Dinarello et al., 2012). Unlike IL-1, no IL-33 signaling complex includes both ST2 and the shared co-receptor IL-1RAcP, hampering the tailored development of biologics for the treatment of IL-33-mediated pathologies. Here, we present the X-ray crystal structure of the ternary IL-33:ST2:IL-1RAcP signaling complex, as well as comprehensive mutational, biophysical, and functional analyses of the IL-33 and IL-1β signaling complexes. Our data define the molecular basis of IL-1RAcP receptor sharing and show that although IL-1RAcP uses the same structural motifs to engage different cytokine-receptor pairs, the mechanisms by which signaling-competent ternary complexes form are distinct.

RESULTS

Signaling Complexes in the IL-1 Family Adopt a Conserved Supramolecular Architecture

We crystallized the ternary complex of murine IL-33:ST2:IL-1RAcP (Figure 1A and Table S1) and determined its 2.8 Å resolution structure. The overall structure resembled those of other ternary complexes from the IL-1 family (Thomas et al., 2012; Tsutsumi et al., 2014; Wang et al., 2010) (Figure 1B). The three ST2 immunoglobulin (Ig) domains wrapped around IL-33. This binary complex was then bound by the co-receptor IL-1RAcP, whose second and third Ig domains (D2 and D3, respectively) engaged a combined interface between ST2 and IL-33. D1 domains from neither ST2 nor IL-1RAcP participated in complex formation.

Although our murine ternary IL-33:ST2:IL-1RAcP complex is similar to the binary human IL-33:ST2 complex (Liu et al., 2013) with an overall root-mean-square deviation (RMSD) of 1.46 Å (Figure S1A), the orientation of the three domains of ST2 differed

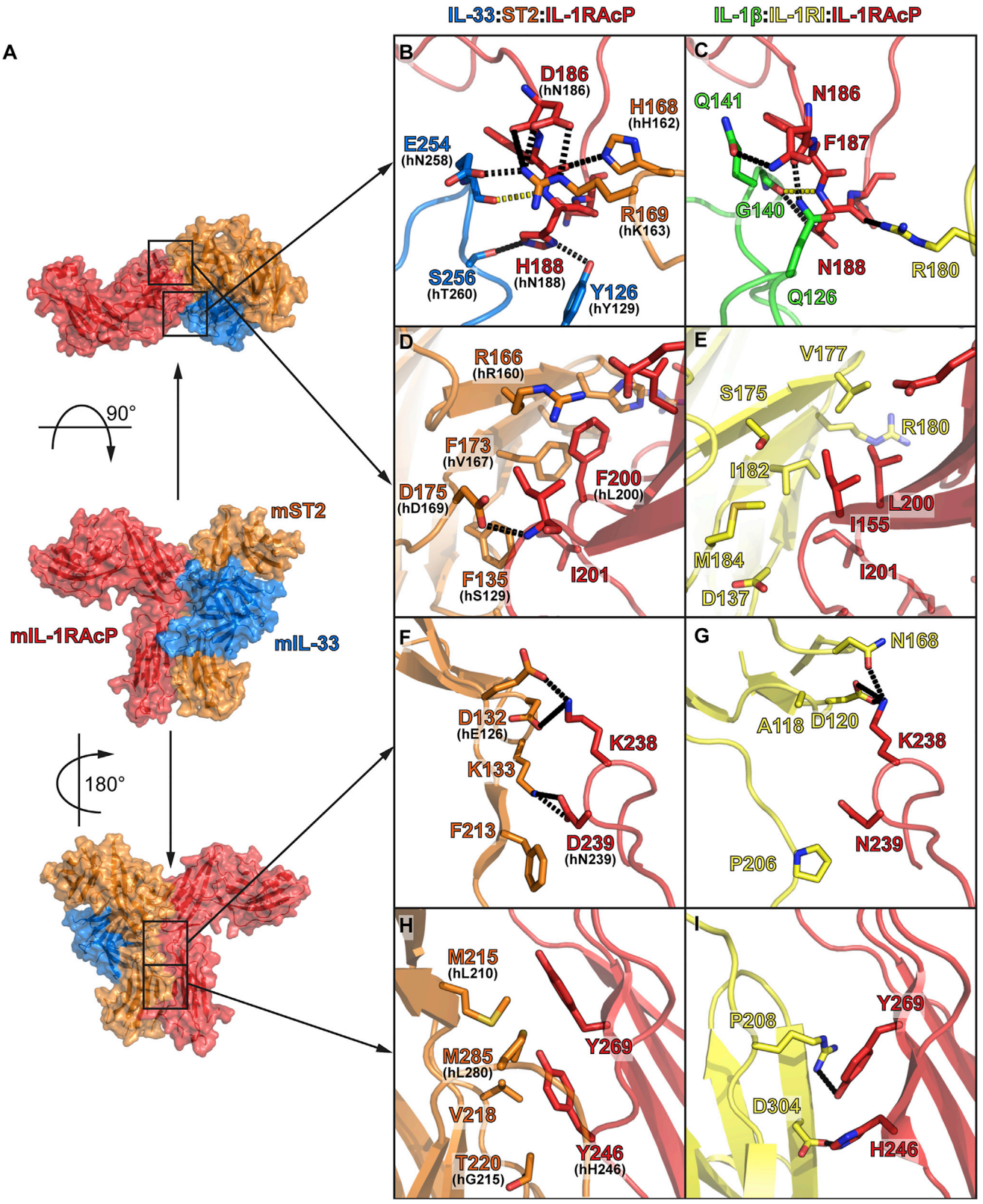

(legend on next page)

between the two complexes, and subsequently, the structures of the individual domains were more conserved than that of the entire binary complex, as indicated by lower RMSD values of the individual domains and cytokine (D1D2: 0.96 Å; D3: 0.94 Å; IL-33: 1.1 Å) than of the entire complex (Figure S1A). D1D2 and D3 of ST2 were shifted in relation to IL-33 upon IL-1RAcP binding (Figure S1A). The ST2 D1 and D2 domains were rotated 4.5°, bringing the backside of ST2 closer to IL-1RAcP (e.g., human ST2 residue D169 [$hST2_{D169}$], which is mouse $mST2_{D175}$, moved 2 Å toward IL-1RAcP), and the ST2 D3 domain was rotated 9°, causing a shift of D3 along the IL-1RAcP-D3 interface (e.g., $hST2_{L233}$ [$mST2_{I238}$] moved 4 Å along IL-1RAcP) (Figure S1A).

The most substantial differences existed at the IL-33:IL-1RAcP interface. The loops connecting β strands 4 and 5 (β4-5 loop) and 11 and 12 (β11-12 loop) were absent in the IL-33:ST2 binary structure, most likely as a result of their inherent flexibility in the absence of IL-1RAcP; these loops also appear to be unstructured in the nuclear magnetic resonance (NMR) structure of IL-33 (Lingel et al., 2009). In the ternary complex structure, conversely, loops β4-5 and β11-12 were both ordered, and the latter made contacts with both IL-1RAcP (201 $Å^2$ buried surface area [BSA]) and ST2 (54 $Å^2$) (Figure 1A). Similar movements were observed between the IL-1β:IL-1RI binary (Vigers et al., 1997) and the IL-1β:IL-1RI:IL-1RAcP ternary complex structures. The overall RMSD of IL-1β:IL-1RI was 1.21 Å, but the relative orientation of the individual domains differed, as evidenced by lower RMSD values of individual domains (D1D2: 0.78 Å; D3: 0.59 Å; IL-1β: 0.8 Å). However, the rotations of the receptor domains differed between the IL-1β and IL-33 complexes (Figure S1B). The IL-1RI D1 and D2 domains shifted on the upper surface of IL-1β by a rotation of 3.7°, in effect causing an upward shift of these domains in relation to the IL-1RAcP binding site (e.g., $IL\text{-}1RI_{N154}$ was displaced by 1.8 Å). The IL-1RI D3 domain rotated around 6.6° toward IL-1RAcP, shifting the receptor D3 domain along the co-receptor and displacing $IL\text{-}1RI_{E234}$ by 3.2 Å. These movements allowed for a closer apposition of the D3 domains of both receptors.

In the crystallographically defined ternary complexes in the IL-1 family, the total BSA at the interface formed by the co-receptor (e.g., IL-1RAcP or IL-18Rβ) and the binary complex of interleukin and primary receptor (e.g., IL-33:ST2, IL-1β:IL-1RI, IL-1β:IL-1RII, or IL-18:IL-18Rα) varied from 2,380 $Å^2$ for the IL-18 complex to 3,718 $Å^2$ for the IL-33 complex (Figure 1C). Although the IL-33:ST2 complex exhibited the largest combined interface with IL-1RAcP, the BSA contributed by the cytokine itself was the least out of all analyzed complexes. Despite this, a conservation of the size of the interface between IL-1RAcP and the individual binary complexes was evident. In all five complexes, the differences in BSA derived mainly from the contribution of the receptor D3 domain. Superposition of the ST2 and IL-1RI D3 domains within their respective ternary complexes indicated that they were rotated with respect to each other by 64° and thereby engaged the IL-1RAcP D3 domain with a different face of the cognate receptor D3 (Figure 1D). This was not caused by IL-1RAcP binding given that the ST2 D3 domain exhibited the same orientation in the binary complex (Figure S1A). Because Ig domains are ellipsoidal, this enabled the broader side of ST2 D3 to engage the common surface of IL-1RAcP D3, resulting in a larger interface than for the IL-1β complex.

Despite these differences, we observed common principles in how the binary cytokine-receptor complex engaged the shared co-receptor IL-1RAcP. First, the loop connecting strands c and d of the D2 domain (c2-d2 loop) resided at the intersection of all three binding partners and exhibited conformational plasticity to accommodate differences in the binary complexes of distinct primary receptors and cytokines (Figure S1C). In the IL-1β:IL-1RI:IL-1RAcP and IL-33:ST2:IL-1RAcP complexes, the c2-d2 loop engaged both the cytokine and receptor through an extensive hydrogen-bonding network (Figures 2A–2C and Figure S2). Second, a hydrophobic patch on the receptor side engaged $IL\text{-}1RAcP_{I155}$ (Figures 2D and 2E). In the IL-1β complex, it made mainly hydrophobic interactions with the two side chains of $IL\text{-}1RI_{I182}$ and $IL\text{-}1RAcP_{I155}$ (Figure 2E). In contrast, in the IL-33 complex, the side chain of $ST2_{D175}$ made van der Waals contacts with the side chain of $IL\text{-}1RAcP_{I155}$ and formed an additional hydrogen bond to the main chain of the same residue (Figure 2D). Third, the IL-1RAcP D2D3 linker engaged the cognate receptors (Figures 2F and 2G). In the IL-1β complex, $IL\text{-}1RAcP_{K238}$ bound $IL\text{-}1RI_{D120}$ through a salt bridge and $IL\text{-}1RI_{N168}$ through a hydrogen bond (Figure 2G). Moreover, it made van der Waals contacts with $IL\text{-}1RI_{A118}$. In addition, there was a contact with the IL-1RI-D2:D3 linker via van der Waals contacts between $IL\text{-}1RAcP_{N239}$ and $IL\text{-}1RI_{P206}$. Similarly, in the IL-33 complex, $IL\text{-}1RAcP_{K238}$ formed salt bridges with $ST2_{D132}$ and $ST2_{E210}$ and between $IL\text{-}1RAcP_{D239}$ and $ST2_{K133}$ (Figure 2F). There was also a linker-linker contact through van der Waals contacts between the side chain of $IL\text{-}1RAcP_{D239}$ and $ST2_{F213}$.

These three common features involved the D2 modules of the receptor and co-receptor. The rotation of the ST2 D3 domain in relation to IL-1RAcP resulted in a different interface (Figure 1D) than was observed in the IL-1β:IL-1RI:IL-1RAcP complex. Even commonly engaged co-receptor residues (e.g., IL-1RAcPH246 [in mouse IL-1RAcPY246] and IL-1RAcPY269) exhibited different rotamer positions (Figures 2H and 2I),

Figure 2. Conserved Interaction Motifs Enable IL-1RAcP Receptor Sharing

(A) Surface representation of the IL-33:ST2:IL-1RAcP complex (the location of the main interaction site between IL-1RAcP and IL-33:ST2 is indicated).

(B and C) Interaction between the IL-1RAcP c2-d2 loop and the cytokine and primary receptor through extensive hydrogen bonds (black dashed line) in the IL-33:ST2:IL-1RAcP (B) and IL-1β:IL-1RI:IL-1RAcP (C) complexes. The conserved main-chain main-chain hydrogen bond is shown in yellow.

(D and E) Hydrophobic interaction centered around $IL\text{-}1RAcP_{I155}$ in the IL-33:ST2:IL-1RAcP (D) and IL-1β:IL-1RI:IL-1RAcP (E) complexes.

(F and G) Polar interactions between the receptor and the IL-1RAcP D2-D3 linker region in the IL-33:ST2:IL-1RAcP (F) and IL-1β:IL-1RI:IL-1RAcP (G) complexes.

(H and I) Interface between receptor D3 domains in the IL-33:ST2:IL-1RAcP (H) and IL-1β:IL-1RI:IL-1RAcP (I) complexes.

Murine IL-33:ST2:IL-1RAcP is shown in (B), (D), (F), and (H). In the case of non-conservation, the human residue is indicated; human IL-1β:IL-1RI:IL-1RAcP is shown in (C), (E), (G), and (I).

See also Figure S2.

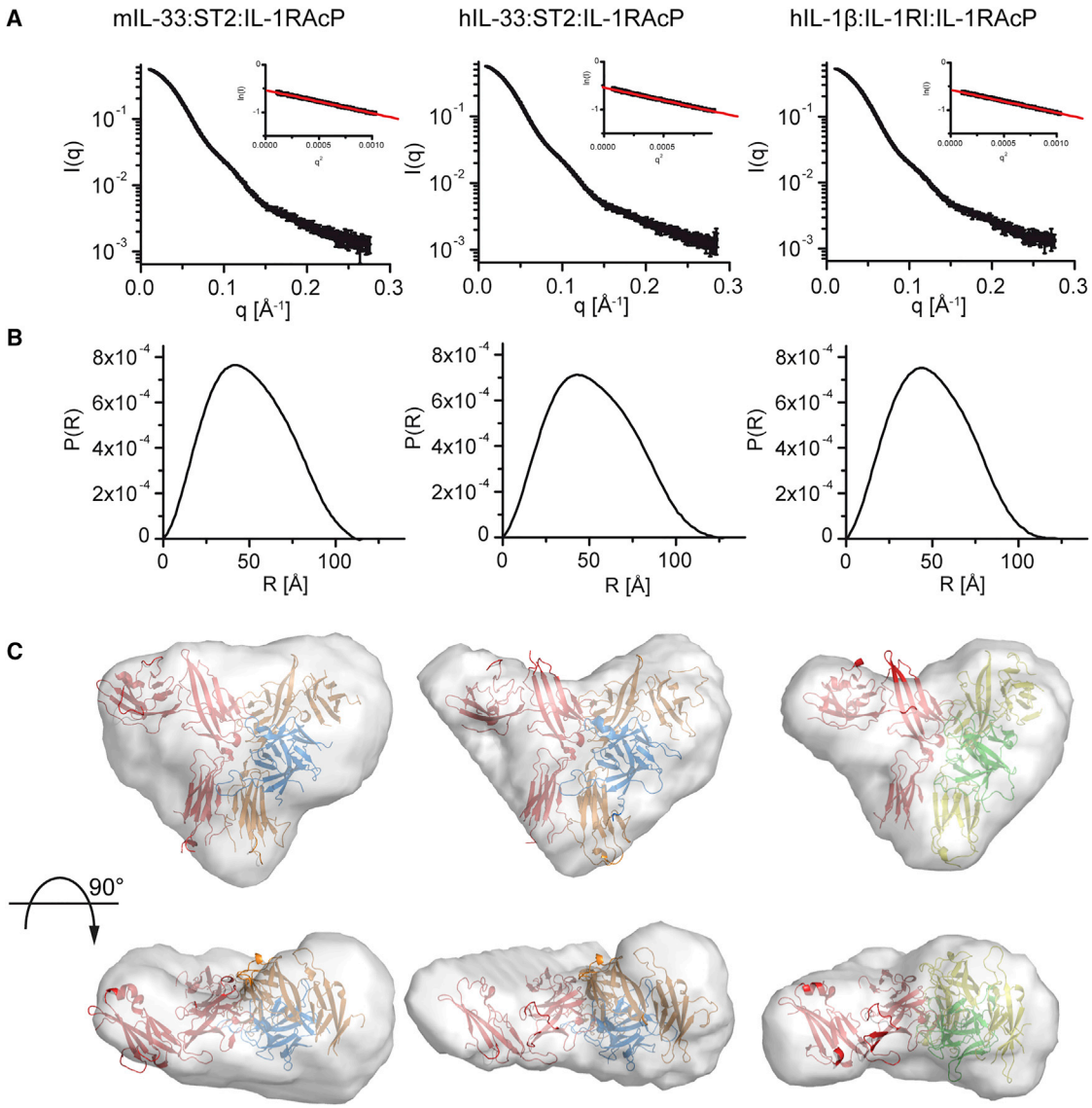

Figure 3. SAXS Studies Confirm Comparability of IL-1 Ternary Complexes in Solution

(A) Scattering profiles of ternary complexes (left, mIL-33:ST2:IL-1RAcP; middle, hIL-33:ST2:IL-1RAcP; right, IL-1β:IL-1RI:IL-1RAcP). Inset shows the fit of the Guinier region of profile and the calculated radius of gyration. A single sample was measured at three different concentrations. Profiles are from highest concentration without signs of aggregation.

(B) Pair-distance distribution function for the three complexes.

(C) *Ab initio* shape reconstruction. Structures of murine IL-33 (left) and human IL-1β (right) ternary complexes were fitted into envelopes calculated from distance distribution plots. The human IL-33 ternary complex (middle) was modeled on the basis of the murine complex structure for IL-33:ST2 and IL-1RAcP from the human IL-1β complex. Colors match those in Figures 1 and 2.

resulting in different engagement of the two receptor D3 surfaces. These receptor surfaces were of a different chemical nature. Although IL-1RAcP$_{H246}$ and IL-1RAcP$_{Y269}$ engaged IL-1RI:D3 through polar interactions (salt bridges to IL-1RI$_{R208}$ and IL-1RI$_{D304}$) (Figure 2I), they used hydrophobic interactions to engage ST2$_{M215}$, ST2$_{V218}$, ST2$_{T220}$, and ST2$_{M285}$ (Figure 2H).

In summary, the IL-33:ST2:IL-1RAcP structure, together with previously determined complex structures involving IL-1RAcP, revealed the conserved usage of structural motifs that can engage diverse cytokine-receptor binary complexes on the co-receptor side through different physicochemical strategies.

Mouse and Human IL-33 Ternary Signaling Complexes Are Indistinguishable in Solution

Mouse and human IL-33, ST2, and IL-1RAcP sequences exhibit a high degree of conservation (Figure S3). To determine whether this translates to similar tertiary and quaternary structures between these sequences, we used small-angle X-ray scattering (SAXS) to analyze the complexes of both human and murine IL-33:ST2:IL-1RAcP, as well as human IL-1β:IL-1RI:IL-1RAcP, in solution. From the scattering profiles (Figure 3A), we calculated pairwise distance distributions (Figure 3B) and generated molecular envelopes of the complexes in solution (Figure 3C).

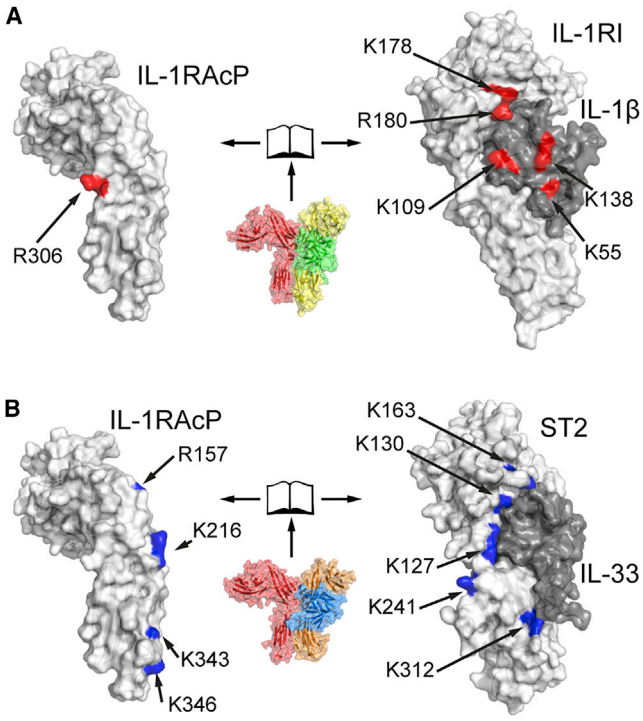

Figure 4. Distinct Engagement of IL-1RAcP by IL-1β:IL-1RI and IL-33:ST2

Analysis of ternary complexes in solution by protein paining identifies sites that are part of the interface between IL-1RAcP and binary cytokine-receptor pairs. (A) Open-book representation of the interface between IL-1RAcP (left) and IL-1β:IL-1RI (right). Interface residues identified through protein painting are colored red.

(B) Same representation for IL-33:ST2:IL-1RAcP as in (A). Identified interface residues are colored blue. See also Figures S4A and S4B. Each complex was analyzed in triplicate, and only sites consistently identified in all replicates are depicted.

The crystal structures of the human IL-1β:IL-1RI:IL-1RAcP and murine IL-33:ST2:IL-1RAcP complexes were superimposable with the respective envelopes derived from SAXS (Figure 3C). Moreover, the SAXS-derived molecular envelope of the human IL-33:ST2:IL-1RAcP complex was superimposable with a model based on our crystal structure of the murine complex (Figure 3C), confirming that the mouse and human IL-33:ST2:IL-1RAcP complexes are largely indistinguishable in solution. Thus, we performed all additional mutational, biophysical, and functional analyses of the IL-33 signaling complex by using human proteins.

IL-33:ST2 and IL-1β:IL-1RI Engage Their Shared Co-receptor, IL-1RAcP, Differently

To interrogate these interfaces in both IL-1β:IL-1RI:IL-1RAcP and IL-33:ST2:IL-1RAcP complexes in more detail, we used protein painting, which involves adding dye molecules that bind protein surfaces with high affinity to a protein complex as well as to its individual components. The bound dye molecules block protease sites, and comparing the generated peptide pattern of the complex with the individual proteins by mass spectrometry can reveal the interface of the complex. Previously, protein painting had been applied to identify a region within the interface of the IL-1β:IL-1RI:IL-1RAcP complex; this region was subsequently targeted with a peptide that disrupted complex formation and signaling (Luchini et al., 2014).

Although the contact sites from protein painting generally confirmed the binding mode of IL-1RAcP with its binary complexes as seen in the crystal structures, these sites were distinctly distributed (Figure 4). For IL-1RAcP in complex with IL-1β:IL-1RI, we confirmed IL-1RAcP$_{R306}$ as the single site identified by protein painting (Luchini et al., 2014). On the receptor side, IL-1RI$_{K178}$ and IL-1RI$_{R180}$ were close to the three-way interface around the IL-1RAcP c2-d2 loop (Figure 2C). As a confirmation of this interface, we identified IL-1β$_{K138}$ within the cytokine β11-12 loop. Moreover, we found IL-1β$_{K55}$ in the β4-5 loop and IL-1β$_{K109}$ in the β8-9 loop to be affected by co-receptor binding. In contrast, in the IL-33:ST2:IL-1RAcP complex, we identified several additional residues in IL-1RAcP as being affected by IL-33:ST2 binding. Residues of IL-1RAcP, including R157, K216, K343, and K346, formed an extended interface arranged along the spine of the co-receptor (Figure 4B). This also corresponded to the pattern observed on ST2, which had five affected residues. Whereas ST2K163 engaged the IL-1RAcP c2-d2 loop (Figure 2B) at the top of the complex, residues K127, K130, K241, and K312 formed an extended interface running down to the D3 domain, which aligned with IL-1RAcP residues R157, K216, K343, and K346 in the ternary complex. No contact regions with IL-1RAcP were identified in IL-33, and likewise, IL-1RAcP$_{R306}$ was not affected by IL-33:ST2 binding. Altogether, the protein-painting analysis suggests that the engagement of the cytokine in the IL-33:ST2 complex is distinct from that in the IL-β:IL-1RI complex.

Kinetic Analysis of Co-receptor Engagement Revealed Differential Usage of Common Motifs in IL-1 and IL-33 Complexes

To gain a more detailed and dynamic view of the interactions between human IL-1β and IL-33 ternary complexes in solution, we conducted hydrogen-deuterium exchange mass spectrometry (HDX-MS), in which the kinetic analysis of deuterium incorporation into the protein complex allows the determination of intrinsic protein flexibility, which can change upon complex formation. In each case, we compared the HDX patterns of the ternary complexes with those of the binary receptor-cytokine complexes and IL-1RAcP alone (Figure 5A). Overall, the data fit the models from the crystal structures well. The interface areas between IL-1RAcP and the two binary complexes contained those peptides that were most protected from deuteration. The peptides with the largest differences between the two states (IL-1RAcP bound versus unbound) on the receptor side were found in the hydrophobic patch region of ST2 (peptide 166–172) and IL-1RI (peptide 129–142, which lay directly below the β strand and contacted the hydrophobic patch on the co-receptor side) (Figure 5B). An IL-1RI peptide containing the residues closest to IL-1RAcP in the crystal structure around IL-1RI$_{I182}$ (Figure 2E) could not be identified during the analysis.

Beyond these similarities of the complexes, peptides derived from cytokine loops β4-5 and β11-12 displayed different exchange behavior. Both IL-1β and IL-33 β4-5 loops exhibited reduced exchange in their respective ternary complexes only at later time points, which indicated that the formation of the

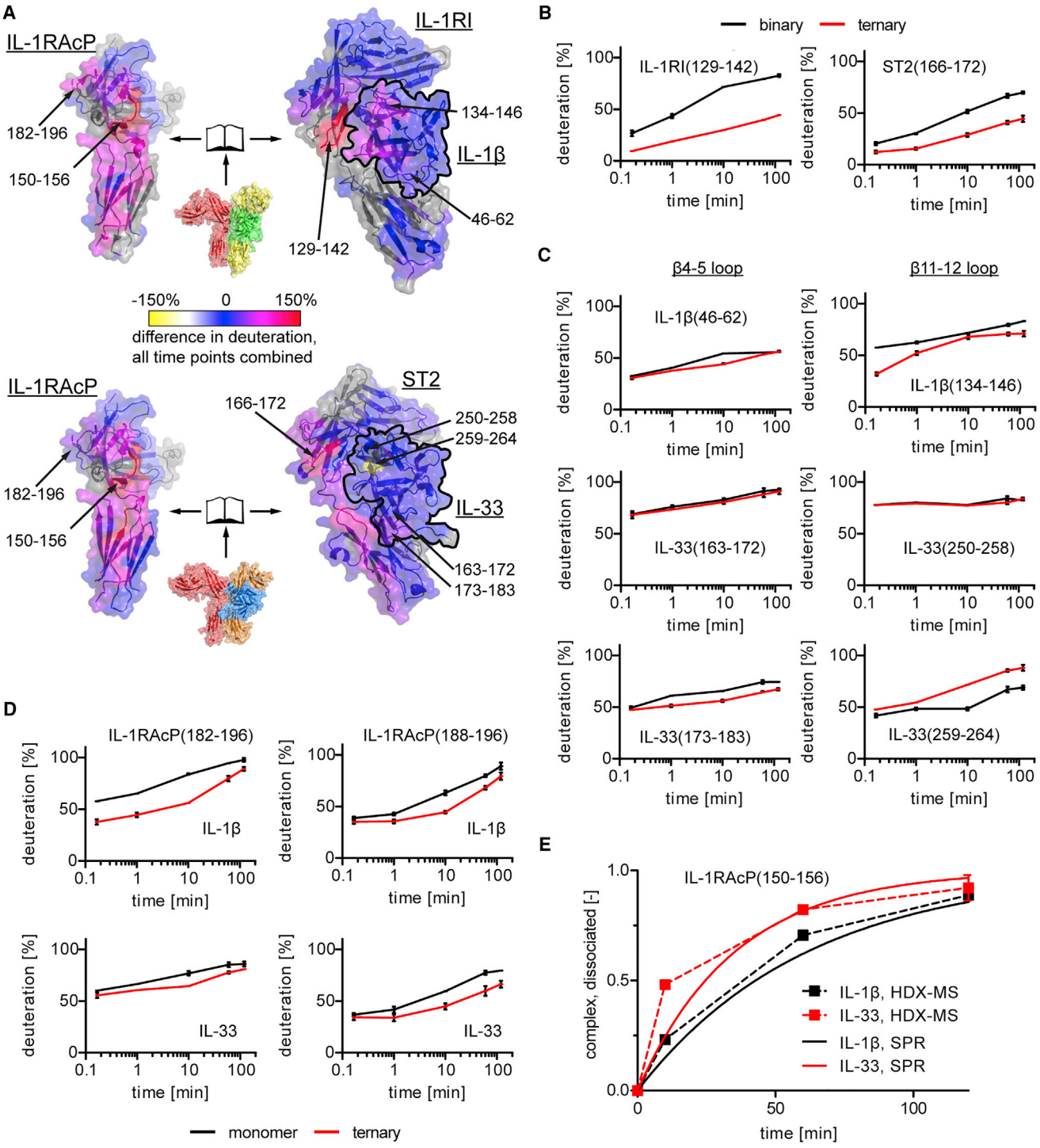

Figure 5. Hydrogen-Deuterium Exchange Mass Spectrometry Reveals Kinetic Behavior of Signaling Complexes in the IL-1 Family

(A) Summary of kinetic analyses. A summation of the observed deuteration differences between ternary complexes and either the IL-1RAcP monomer or the cytokine-primary-receptor binary complex is plotted onto the surface of the IL-1β:IL-1RI:IL-1RAcP (top) and IL-33:ST2:IL-1RAcP (bottom) structures in open-book representation for easy visualization of the interacting surfaces. The cytokine is outlined in black in the binary complexes. Discussed peptides are indicated. Gray areas indicate unidentified peptides.

(B–D) Kinetic traces for peptides in (B) the hydrophobic patch regions of IL-1RI (left) and ST2 (right), (C) the β4-5 (left) and β11-12 (right) loops of IL-1β and IL-33, and (D) the c2-d2 loop of IL-1RAcP. Data represent the average of three independent experiments ± SD.

(E) Comparison of ternary-complex dissociation as observed by HDX-MS (dashed lines) and calculated from SPR analysis (solid lines).

See also Figures S4C and S4D.

ternary complex had some indirect effects on the dynamic behavior of this region (Figure 5C). However, the IL-33 β4-5 loop exhibited a higher percentage of deuteration overall, indicating that this region was more amenable to exchange and suggesting that the β4-5 loop of IL-33 was just as flexible in the ternary complex as it was in both its binary complex (Liu et al., 2013) and unbound (Lingel et al., 2009) forms. In contrast, the β11-12 loop in IL-1β (peptide 134–146) exhibited only half as much deuteration in the ternary complex as in the binary complex at the earliest time point (Figure 5C), indicating that this loop was shielded from greater exchange upon binding the co-receptor and verifying that this region contributed to the engagement of IL-1RAcP (Figure 2C). IL-33 exhibited markedly different behavior. Peptide IL-33(250–258), including two-thirds of the β11-12 loop (IL-33(251–261)), was already highly deuterated at the earliest time point, indicating accessibility of this region even in the ternary complex, and accordingly, this region was not influenced by co-receptor binding (Figure 5C). In contrast, peptide IL-33(259–264), including the remainder of the β11-12 loop, was destabilized in the ternary complex, which showed more HDX than the binary complex (Figure 5C). This suggests that IL-1RAcP binding imposed a change in secondary structure here, an effect not seen for any other region in either complex. We observed similar behavior between peptides IL-1RAcP(182–196) and IL-1RAcP(188–196), which both contain the IL-1RAcP(183–190) peptide in the c2-d2 loop (Figure 5D) that bound to the cytokine β11-12 region (Figures 2B and 2C). Binding of IL-1β:IL-1RI and also of IL-33:ST2 to IL-1RAcP reduced exchange, albeit to a larger extent in the former complex. This indicates that this loop engaged the complex of IL-33:ST2 and IL-1β:IL-1RI in a fashion similar to that seen in the crystal structures (Figures 2B and 2C); however, it made more stable contact in the IL-1β complex, as evidenced by reduced deuterium exchange for peptide IL-1RAcP(182–196) even at the earliest time point. In contrast, the same peptide in the IL-33 ternary complex exhibited no significant differences for the two earliest measurements. In addition, the observed differences could be attributed to the first half of the peptide because peptide IL-1RAcP(188–196) exhibited similar behavior in both ternary complexes (Figure 5D).

The peptide with the highest percentage of protection of hydrogen-deuterium exchange in both complexes was IL-1RAcP(150–156) (Figure S4C), which included IL-1RAcP$_{I155}$ in the hydrophobic patch region of IL-1RAcP (Figures 2D and 2E). This peptide exhibited exchange behavior with EX1 kinetics (Weis et al., 2006) (i.e., the complex dissociation rate was much slower than the exchange rate), which resulted in bimodal mass spectra for this peptide (Figure S4D). Deconvolution of the individual components, which allowed for the determination of the fraction of dissociated—and thus exchanged—peptides (Figure 5E) (Guttman et al., 2013), suggests that the IL-33 ternary complex dissociated faster (half-life of 10 min) than the IL-1β complex (half-life of >30 min). When we measured the binding of both binary complexes to IL-1RAcP by surface-plasmon resonance (SPR) spectroscopy (Table S2), we found that the dissociation rate was faster for the IL-33 ternary complex (2.7×10^{-4} s^{-1}; half-life of 26 min) than for IL-1β (4.7×10^{-4} s^{-1}; half-life of 43 min).The HDX-MS analysis confirmed that IL-1RAcP uses similar motifs to engage IL-1β:IL-1RI and IL-33:ST2 but employs these differently in each complex.

IL-33 Signal Initiation Is Less Cytokine Dependent Than Is IL-1β

To gain a more detailed understanding of the distribution of binding energy within the interfaces of the human IL-1 and IL-33 signaling complexes, we undertook a comprehensive alanine-scanning mutagenesis analysis (Cunningham and Wells, 1989) in which we generated a total of 76 mutants and measured their effects on the binding of the binary complexes to IL-1RAcP by SPR (Figure 6, Figures S5 and S6, and Table S2). This allowed us to clearly identify common IL-1RAcP-binding hotspots that were used for both IL-1β:IL-1RI and IL-33:ST2. In both complexes, IL-1RAcP$_{I155A}$ contributed approximately 4 kcal/mol and IL-1RAcP$_{N189A}$ provided more than 2 kcal/mol of binding energy. These residues were central to two of the common structural features of these signaling complexes (Figures 2B–2E). In contrast to these commonalities, we identified additional hotspots that were unique to either IL-1β:IL-1RI or IL-33:ST2. Residue IL-1RAcP$_{Y269}$ in the D3 domain was important for IL-33:ST2 binding, but this same residue made a negligible energetic contribution to IL-1β:IL-1RI binding. Conversely, IL-1RAcP$_{R306}$, which is a hotspot for IL-1β signaling (Luchini et al., 2014), contributed energetically in a substantial way only to IL-1β:IL-1RI binding. Another residue previously suggested to be important for the formation of ternary complexes is IL-1RAcP$_{S205}$ (Wang et al., 2010), which formed a hydrogen bond to IL-1β$_{D145}$ in IL-1β ternary complexes but contacted neither IL-33 nor ST2 directly in the IL-33:ST2:IL-1RAcP structure (Figure S2C). The binding analysis verified this observation. Mutation of IL-1RAcP$_{S205A}$ influenced binding to IL-1RAcP only by IL-1β:IL-1RI but not by IL-33:ST2.

Furthermore, only a single hotspot on IL-1RI, residue I182, faced the hydrophobic patch around IL-1RAcP$_{I155}$ (Figure 2E). In IL-1β, several residues contributed more than 0.5 kcal/mol of binding energy to complex formation. IL-1β$_{D54}$ and IL-1β$_{K55}$ resided on the β4-5 loop and interacted with IL-1RAcP$_{R306}$. IL-1β$_{I106}$ resided on β strand 8 and made contacts with IL-1RAcP. IL-1β$_{Q126}$ was part of the hydrogen-bonding network that engaged loop c2-d2 in IL-1RAcP (Figure 2C). Finally, IL-1β$_{D145}$, previously identified as important for the agonist function of IL-1β (Ju et al., 1991), interacted with IL-1RAcP$_{S205}$.

In contrast to IL-1RI, which showed a very narrow spatial distribution of binding energy, ST2 exhibited a much broader distribution with more contributing residues (Figure 6D). Of the residues that exhibited substantial effects on binding energy, ST2$_{H162}$ and ST2$_{K163}$ coordinated loop c2-d2 of IL-1RAcP (Figure 2B), and residues ST2$_{F165}$, ST2$_{V167}$, and ST2$_{D169}$ were all part of the hydrophobic patch that faced IL-1RAcP$_{I155}$ (Figure 2D). Residues ST2$_{F208}$ and ST2$_{L210}$ faced residue IL-1RAcP$_{Y269}$ in the D3 domain (Figure 2H). Also, the hydrogen bond between residues ST2$_{K127}$ and IL-1RAcP$_{N239}$ in the D2D3 linker region contributed to binding (Figure 2F). The alanine-scanning mutagenesis analysis of IL-33 revealed no pronounced hotspots (Figure 6E). Of all mutants that we analyzed, IL-33$_{D175A}$ exhibited the largest effect on binding; it resided in the β4-5 loop and formed a hydrogen bond through its main chain to IL-1RAcP$_{S303}$ (Figure S2B).

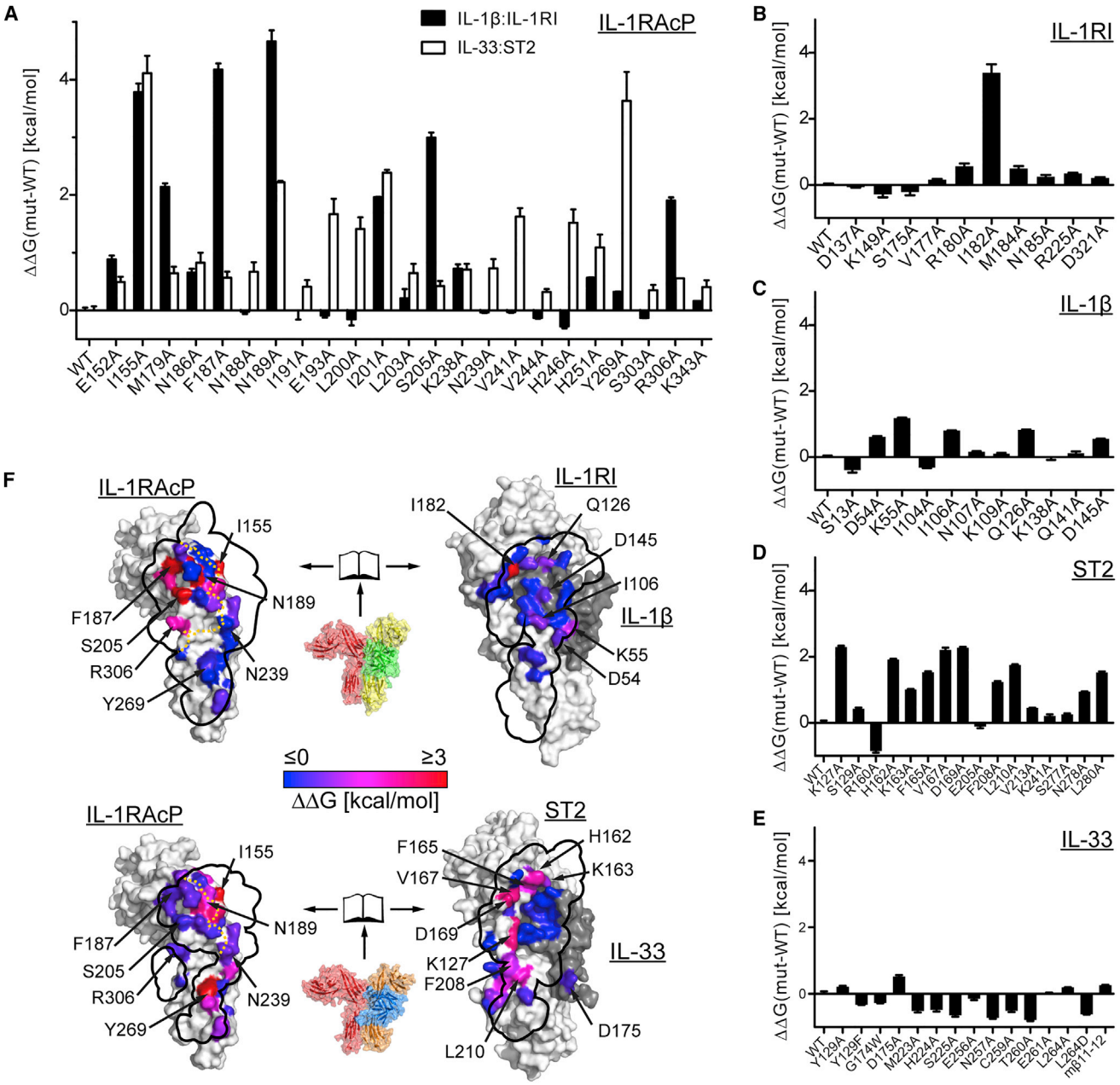

Figure 6. Binding Analysis of IL-1 Signaling Complexes Reveals Differential Distribution of Binding Energies at Interfaces with IL-1RAcP

(A–E) Affinities for the interaction between the IL-1β:IL-1RI or IL-33:ST2 complex and IL-1RAcP (mutants and wild-type) were measured by SPR and converted to differences in binding free energy with the formula $\Delta\Delta G = R \times T \times \ln(K_{D,mut}/K_{D,WT})$. Values represent the average of at least three independent experiments. Error bars represent SEM. (A) Analysis of IL-1RAcP mutants for binding to either IL-1β:IL-1RI or IL-33:ST2. (B–E) Analysis of IL-1RI (B), IL-1β (C), ST2 (D), and IL-33 (E) mutants.

(F) Results of binding analysis are plotted onto crystal structures. Top: the IL-1β ternary complex is rendered as a surface in open-book representation for easy visualization of the binding interface. Mutated residues are colored according to their change in binding free energy, ΔΔG. The corresponding interface from the other half of the complex is indicated with a black outline. In the case of the binary-complex outline on IL-1RAcP (left), the approximate separation between cytokine and receptor is indicated in orange. Bottom: same analysis for the IL-33 ternary complex.

See also Figures S5 and S6.

In total, the alanine-scanning mutagenesis analysis revealed two common mechanisms in IL-1RAcP engagement: (1) the mainly hydrophobic interaction around IL-1RAcP$_{I155}$, which included a conserved hydrophobic spot on the primary receptor side, and (2) the coordination of IL-1RAcP loop c2-d2 by the cytokine and primary receptor, mainly through an extended hydrogen-bond network. However, whereas the first was equally important for IL-1β:IL-1R1 and IL-33:ST2 binding to IL-1RAcP,

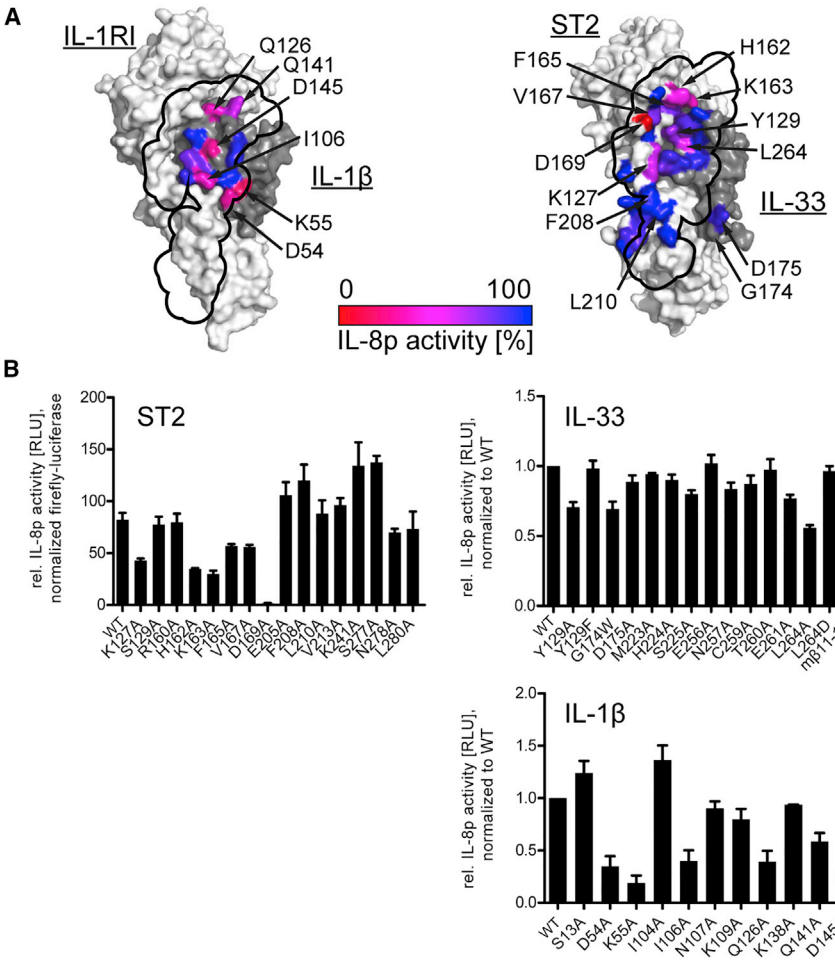

Figure 7. IL-33 Signaling Depends Less on Direct Cytokine-Co-receptor Interactions Than Does IL-1β

Signaling was assessed in HEK293T-based reporter cells containing an IL-8 promoter-driven luciferase. Cells were activated with either 5 pM IL-33 or 100 pM IL-1β, and luciferase activity was measured 5 hr after stimulation.

(A) The location of mutants at the IL-1RAcP interface is indicated on the binary cytokine-receptor surfaces (left, IL-1β:IL-1RI; right, IL-33:ST2) and colored according to how their activity relates to that of wild-type signaling. The binding site of IL-1RAcP is projected onto the binary cytokine-receptor surface (black outline).

(B) Signaling-assay results that form the basis for the coloring in (A). For ST2 mutants (upper left), data were normalized to those of co-transfected, constitutively active firefly luciferase for transfection efficiency. For analysis of cytokine mutants (IL-33 in the upper right and IL-1β in the lower right), results were normalized to those of wild-type cytokines. Data represent the average of three independent experiments, each conducted in triplicate. Error bars represent SEM.

the latter contributed mainly to binding of IL-1β:IL-1RI to IL-1RAcP. In contrast, IL-33:ST2 had more contacts of energetic importance with IL-1RAcP in the interface formed by their D3 domains.

IL-33 Signaling Depends Less on Direct Cytokine-Co-receptor Interactions Than Does IL-1β Signaling

We next determined whether the observed differences in binding affinity translated to differences in signaling. We observed a significant reduction in hIL-33-mediated signaling for ST2 mutants K127A, H162A, K163A, and D169A, the latter of which exhibited the largest reduction in signaling (Figure 7). This was in line with the observations from the direct binding assay. However, we found that none of the interactions between the D3 domains of ST2 and IL-1RAcP had a substantially negative effect on signaling.

In accordance with the observations from the binding assay, few mutations in IL-33 had an effect on signaling. Mutations with the clearest reduction in signaling in comparison with that of wild-type IL-33 included IL-33 mutants Y129A, G174W, and L264A. Whereas IL-33_{Y129A} exhibited reduced ST2 activation, the corresponding mutant IL-33_{Y129F} showed normal activation, specifically implicating its aromatic ring in potentially stabilizing the IL-33 β11-12 loop by packing against it (Figure 2B). The mutation with the largest reduction in binding affinity, IL-33_{D175A}, did not show a substantial reduction in activation. However, introduction of a bulky side chain at the previous residue in the IL-33 β4-5 loop by mutation IL-33_{G174W} might have influenced the flexibility of this region and thereby the interaction with IL-1RAcP, although this effect was seen only in signaling but not binding. Finally, IL-33_{L264A} exhibited the largest reduction in signal activation. This residue did not make direct contact with IL-1RAcP. However, it sat underneath the IL-33 β11-12 loop and might have influenced its conformation (Figure S2C).

In contrast, in the IL-1β complex, the corresponding residue, IL-$1β_{D145}$, formed a hydrogen bond to IL-$1RAcP_{S205}$. This residue is important for IL-1β activity (Ju et al., 1991; Wang et al., 2010) (and also Figures 6C and 7B). In the IL-33 complex, both residues were much farther apart (11.4 Å between both Cα atoms) than in the IL-1β complex (7.7 Å). Reverting this residue in IL-33 to aspartate (IL-33_{L264D}), as found in IL-1β, restored IL-33 activity (Figure 7B), indicating either that IL-33 can approach IL-1RAcP more closely than observed in the crystal structure to form the hydrogen bond seen in the IL-1β complex or that this residue is important for stabilization of the β11-12 loop and that IL-33_{L264D} can be substituted without significant effects on signaling. The β11-12 loop is one of the most divergent areas between human and murine IL-33 in both sequence and length (Figure S3), a quality that makes it difficult to exactly predict its molecular interactions with IL-1RAcP on the basis of the murine complex structure. To assess the potential differences, we substituted the murine β11-12 loop for the human loop in human IL-33 (IL-$33_{mβ11-12}$) and observed a reduction in signaling. Considering that we saw an increase in flexibility in this region

by HDX-MS (Figure 5C), the chimeric protein could have altered flexibility in this region to make productive engagement of IL-1RAcP more difficult. No other IL-33 mutations of interface residues affected signaling substantially.

Mutants of IL-1β exhibited larger losses in signaling than mutants of Il-33 (Figure 7). The same mutations that had the largest effects on binding (Figure 6) also showed the largest reductions in signal activation. For example, IL-1β_{D54A} and IL-1β_{K55A} on the β4-5 loop exhibited the largest reduction. Also, IL-1β_{D145A} in the extension of the β11-12 loop (Figure S2C) exhibited reduced signaling through IL-1RI. Together, these data confirm the direct contribution of individual residues of IL-1β to signaling, whereas IL-33 signaling depended less on single residues contacting hIL-1RAcP than on an interface that was more distributed (Figure S7).

DISCUSSION

Through combined structural, molecular, and functional approaches, we discerned the basis for sharing the main co-receptor in the IL-1 family, IL-1RAcP. Our data allowed us to define several conserved interaction motifs between the shared receptor IL-1RAcP and its binary cytokine-receptor complexes, including (1) loop c2-d2 of IL-1RAcP, which forms a cytokine-sensor loop that engages both the cytokine and its primary receptor; (2) residue IL-1RAcP$_{I155}$, which acts as a hydrophobic hook; and (3) polar interactions between the primary receptor and the linker region between domains 2 and 3 of IL-1RAcP. Also, the D3 domains of both receptors engaged each other by using similar contact points on the co-receptor side, although they employed markedly different chemical strategies on the receptor side.

The molecular basis for receptor sharing by the IL-1 family of cytokines can be compared according to the principles governing receptor sharing for other major cytokine families. The previous comparison of the signaling complex IL-1β:IL-1RI:IL-1RAcP with the non-signaling complex IL-1β:IL-1RII:IL-1RAcP suggests the use of disparate interactions for complex formation with the exception of the hydrophobic patch around IL-1RAcP$_{I155}$ and IL-1RAcP$_{I201}$ (Thomas et al., 2012). With the IL-33:ST2:IL-1RAcP signaling complex, we have demonstrated that the interface contains additional shared motifs, and although overlap exists in the engagement of residues in the receptor D3 domains, the chemical nature of these interactions is distinct. Within the common γ-chain cytokines, shape complementarity and stem-loop contacts between the two membrane-proximal receptor domains seem to enable receptor sharing (Wang et al., 2009). Receptor sharing of gp130, in contrast, relies more on the recognition of different cytokine surfaces through chemically unique interactions. Additionally, within the interferon family, type I interferons engage their receptor through common anchor points (Thomas et al., 2011). Recently, the structure of an affinity-enhanced type II interferon (IFN-λ) with the IFN-λ-specific receptor IFN-λR1 and its co-receptor IL-10Rβ, which is shared between several cytokines in the IL-10 superfamily, revealed the similar use of anchor points on the co-receptor to engage several distinct cytokines (Mendoza et al., 2017).

Although IL-1RAcP employed a virtually unchanged interface to engage two largely distinct binary cytokine-receptor pairs, it used the same residues as anchor points. A starkly distinguishing factor was the contribution of IL-1β and IL-33 to complex stability and signaling (Figure S7). Whereas IL-1β contributed almost half of the BSA to the interface with IL-1RAcP, IL-33 provided roughly a quarter, which was reflected in the energetic contributions of IL-1β and IL-33 to binding and complex stability. It appeared that the major influence of IL-33 on signaling activation occurred through stabilization of ST2 in a conformation that was compatible with IL-1RAcP binding. Indeed, the relative orientation of the primary receptor D1D2 and D3 domains was highly flexible in the absence of cytokine. For ST2, this has been shown experimentally (Liu et al., 2013) and through modeling (Yang et al., 2016). Upon IL-33 binding, a single conformation is stabilized (Liu et al., 2013). Although IL-1RI is similarly stabilized in a single conformation by IL-1β binding, the major influence on ternary complex formation and signaling activation in this case was proper presentation of this cytokine to IL-1RAcP by its cognate receptor, such that the cytokine could be involved in nearly all important interactions. In contrast to the cognate receptors, IL-1RAcP exhibits much less flexibility (Liu et al., 2013), most likely because its D2 and D3 domains are closer to the linker between them (Wang et al., 2010).

Although ST2 made extensive contacts with IL-1RAcP through its D3 domain, and although these contacts proved to be important for complex stability, they appeared to be unimportant for signaling in our assays. At least in the context of the full-length receptors, the binding interface formed in the membrane-distal part of the receptor complex exhibited elevated importance, meaning that the restricted diffusion of the full-length receptor in the cell membrane might compensate for the affinity loss that was measured for the soluble proteins. Also, we almost exclusively measured the effect of single mutations, whereas combinatorial mutants might lead to more noticeable changes in signaling. In other receptor systems, changes in binding affinities likewise do not always correlate with signaling outcomes. Similar to IL-4 variants (Junttila et al., 2012), IL-13 variants engineered to span several orders of magnitude of affinity reveal a "buffering zone" where increases in complex stability do not correlate with increased signaling potency (Moraga et al., 2015). Modeling suggests that receptor endocytosis becomes the rate-limiting step for activation (Moraga et al., 2015) in these cases.

Together with the observation that the region around IL-1RAcP$_{I155}$ exhibited a dissociation rate of the complex on the same timescale as the overall rate measured by SPR, the negligible contribution of IL-33 to co-receptor binding suggests that a stepwise process for the formation of ternary complexes leads to productive signaling. First, the cytokine binds its primary receptor, thereby stabilizing the arrangement of its D1D2 and D3 domains in an IL-1RAcP-receptive manner. Then, this binary complex engages IL-1RAcP, most likely through initial long-range electrostatic interactions (Selzer et al., 2000). Subsequently, the hydrophobic hook around IL-1RAcP$_{I155}$ engages the corresponding patch on the receptor side before the cytokine-sensor loop (IL-1RAcP c2-d2 loop) binds at the seam of the cytokine and primary receptor. This causes the D3 domains to zipper up. These binding steps ultimately cause the intracellular receptor TIR domains to be positioned closely enough to form a platform for MyD88 recruitment and signal initiation through the Myddosome (Vyncke et al., 2016).

The antagonistic activity of IL-1Ra can be attributed at least in part to its distinct loops facing the co-receptor binding site, and the swapping of these loops into IL-1β drastically reduces the affinity of a binary complex to IL-1RAcP. This highlights the importance of the IL-1 agonist cytokine in recruitment of IL-1RAcP. In contrast, no antagonistic cytokine has been described to directly counteract IL-33 signaling. Given that IL-33-mediated signal activation relies mainly on the stabilization of ST2, this is expected. For IL-33, the main regulation of cytokine signaling on the receptor level happens through the alternatively spliced receptor sST2, which acts as a decoy receptor. In contrast, at least one bona fide antagonist, IL-36Ra, exists for the IL-36 subfamily, the third set of IL-1RAcP-dependent cytokines in the IL-1 family (Günther and Sundberg, 2014; Towne et al., 2011), and we expect that in these cases the agonistic cytokines IL-36α, IL-36β, and IL-36γ will also make larger contributions to co-receptor binding than will IL-33.

We focused our comparison of IL-33:ST2 to IL-1β:IL-1RI because these represent the biophysically best-characterized molecules in the IL-1 family. Biologically, however, IL-1α is more closely related to IL-33 than to IL-1β. Like IL-33, IL-1α is recruited to the cell nucleus and only released upon cell stress, when it acts as an alarmin (Rider et al., 2013). And like IL-33, IL-1α has activity in its precursor form, but its activity is augmented by protease processing. Whether this relationship extends to the molecular mechanism by which the IL-1α signaling complex is formed remains to be seen.

IL-37, another IL-1 cytokine with nuclear translocation, has anti-inflammatory properties via interaction with IL-18Rα and SIGIRR (IL-1R8) (Nold-Petry et al., 2015). SIGIRR has also been demonstrated to negatively regulate IL-33:ST2 signaling (Bulek et al., 2009), raising the intriguing possibility that IL-33 can also recruit SIGIRR as an alternative co-receptor to negatively regulate inflammation.

Evolution of the IL-1 family provides insight into distinct dependencies on antagonistic cytokines or decoy receptors. IL-33 evolved with placental mammals, given that it is not found in birds, and is an evolutionarily younger protein (Sattler et al., 2013) than IL-1β. In contrast, ST2 orthologs have been found in mammals and in both birds and fish, indicating a more ancient role independent of IL-33. Moreover, there is evidence of sST2 function independent of IL-33 (e.g., in liposaccharide-induced monocyte and dendritic cell activation; Nagata et al., 2012; Takezako et al., 2006), and full-length ST2 has been shown to inhibit TLR4 signaling via recruitment of commonly used adaptor proteins containing TIR domains (Brint et al., 2004). With no antagonistic cytokine for ST2 and only a single agonistic cytokine available, no evolutionary pressure exists for IL-1RAcP to distinguish between different ST2-bound cytokines, potentially explaining why IL-33-mediated signal activation depends more on ST2 than on IL-33. In contrast, IL-1RI and IL-36R each have several agonists and at least one antagonist, and thus cytokine contributions dominate.

Finally, IL-33 signaling is an attractive therapeutic target for many indications (Liew et al., 2016). Our results suggest that targeting IL-33 directly might prove less effective than targeting its cognate or co-receptors. Moreover, the identification of common and distinct hotspots for the binary complexes of IL-1β:IL-1RI and IL-33:ST2 on IL-1RAcP will help enable the targeted development of biologics that could block these signaling pathways either simultaneously or independently, depending on the desired clinical outcome.

STAR★METHODS

Detailed methods are provided in the online version of this paper and include the following:

- KEY RESOURCES TABLE
- CONTACT FOR REAGENT AND RESOURCE SHARING
- EXPERIMENTAL MODEL AND SUBJECT DETAILS
- METHOD DETAILS
  - Plasmids and Proteins
  - Protein Expression and Purification
  - Crystallization and Structure Determination
  - Small Angle X-Ray Scattering (SAXS)
  - Direct Binding Analysis
  - Signaling Studies
  - Hydrogen-Deuterium-Exchange Mass Spectrometry
  - Protein-Painting by Mass Spectrometry
- QUANTIFICATION AND STATISTICAL ANALYSIS
- DATA AND SOFTWARE AVAILABILITY

SUPPLEMENTAL INFORMATION

Supplemental Information includes seven figures and two tables and can be found with this article online at http://dx.doi.org/10.1016/j.immuni.2017.08.004.

AUTHOR CONTRIBUTIONS

S.G. and E.J.S. conceived the project and wrote the manuscript. S.G. crystallized and solved crystal structure and conducted SAXS, SPR, and signaling experiments. D.D. performed HDX-MS experiments. A.L. conducted the protein painting study. A.L.B. and R.B. provided reagents. A.L.B. contributed to SPR experiments. D.A.B. contributed to SAXS experiments. P.W., L.L., and E.J.S. supervised the research.

ACKNOWLEDGMENTS

These studies were supported by an American Asthma Foundation Scholar Award (13-0066) to E.J.S. and National Institutes of Health (NIH) awards (R01AR068436 and R33CA206937) to L.L. This research used resources of the Advanced Photon Source, operated for the Department of Energy Office of Science by Argonne National Laboratory under contract no. DE-AC02-06CH11357, and the Cornell High Energy Synchrotron Source, supported by National Science Foundation award DMR-0936384 and NIH award GM-103485. This work was supported in part by the University of Maryland School of Pharmacy Mass Spectrometry Center (SOP1841-IQB2014).

Received: April 17, 2017
Revised: June 27, 2017
Accepted: August 11, 2017
Published: September 19, 2017

REFERENCES

Acerbo, A.S., Cook, M.J., and Gillilan, R.E. (2015). Upgrade of MacCHESS facility for X-ray scattering of biological macromolecules in solution. J. Synchrotron Radiat. *22*, 180–186.

Adams, P.D., Afonine, P.V., Bunkóczi, G., Chen, V.B., Davis, I.W., Echols, N., Headd, J.J., Hung, L.W., Kapral, G.J., Grosse-Kunstleve, R.W., et al. (2010).

PHENIX: a comprehensive Python-based system for macromolecular structure solution. Acta Crystallogr. D Biol. Crystallogr. *66*, 213–221.

Aricescu, A.R., Lu, W., and Jones, E.Y. (2006). A time- and cost-efficient system for high-level protein production in mammalian cells. Acta Crystallogr. D Biol. Crystallogr. *62*, 1243–1250.

Bessa, J., Meyer, C.A., de Vera Mudry, M.C., Schlicht, S., Smith, S.H., Iglesias, A., and Cote-Sierra, J. (2014). Altered subcellular localization of IL-33 leads to non-resolving lethal inflammation. J. Autoimmun. *55*, 33–41.

Bonilla, W.V., Fröhlich, A., Senn, K., Kallert, S., Fernandez, M., Johnson, S., Kreutzfeldt, M., Hegazy, A.N., Schrick, C., Fallon, P.G., et al. (2012). The alarmin interleukin-33 drives protective antiviral CD8$^+$ T cell responses. Science *335*, 984–989.

Brint, E.K., Xu, D., Liu, H., Dunne, A., McKenzie, A.N., O'Neill, L.A., and Liew, F.Y. (2004). ST2 is an inhibitor of interleukin 1 receptor and Toll-like receptor 4 signaling and maintains endotoxin tolerance. Nat. Immunol. *5*, 373–379.

Bulek, K., Swaidani, S., Qin, J., Lu, Y., Gulen, M.F., Herjan, T., Min, B., Kastelein, R.A., Aronica, M., Kosz-Vnenchak, M., and Li, X. (2009). The essential role of single Ig IL-1 receptor-related molecule/Toll IL-1R8 in regulation of Th2 immune response. J. Immunol. *182*, 2601–2609.

Carriere, V., Roussel, L., Ortega, N., Lacorre, D.A., Americh, L., Aguilar, L., Bouche, G., and Girard, J.P. (2007). IL-33, the IL-1-like cytokine ligand for ST2 receptor, is a chromatin-associated nuclear factor in vivo. Proc. Natl. Acad. Sci. USA *104*, 282–287.

Cayrol, C., and Girard, J.P. (2009). The IL-1-like cytokine IL-33 is inactivated after maturation by caspase-1. Proc. Natl. Acad. Sci. USA *106*, 9021–9026.

Cayrol, C., and Girard, J.P. (2014). IL-33: an alarmin cytokine with crucial roles in innate immunity, inflammation and allergy. Curr. Opin. Immunol. *31*, 31–37.

Cohen, E.S., Scott, I.C., Majithiya, J.B., Rapley, L., Kemp, B.P., England, E., Rees, D.G., Overed-Sayer, C.L., Woods, J., Bond, N.J., et al. (2015). Oxidation of the alarmin IL-33 regulates ST2-dependent inflammation. Nat. Commun. *6*, 8327.

Cunningham, B.C., and Wells, J.A. (1989). High-resolution epitope mapping of hGH-receptor interactions by alanine-scanning mutagenesis. Science *244*, 1081–1085.

Dinarello, C.A., Simon, A., and van der Meer, J.W. (2012). Treating inflammation by blocking interleukin-1 in a broad spectrum of diseases. Nat. Rev. Drug Discov. *11*, 633–652.

Emsley, P., Lohkamp, B., Scott, W.G., and Cowtan, K. (2010). Features and development of Coot. Acta Crystallogr. D Biol. Crystallogr. *66*, 486–501.

Evans, P.R., and Murshudov, G.N. (2013). How good are my data and what is the resolution? Acta Crystallogr. D Biol. Crystallogr. *69*, 1204–1214.

Franke, D., and Svergun, D.I. (2009). DAMMIF, a program for rapid ab-initio shape determination in small-angle scattering. J. Appl. Cryst. *42*, 342–346.

Goujon, M., McWilliam, H., Li, W., Valentin, F., Squizzato, S., Paern, J., and Lopez, R. (2010). A new bioinformatics analysis tools framework at EMBL-EBI. Nucleic Acids Res. *38*, W695–W699.

Guan, Y., Pazgier, M., Sajadi, M.M., Kamin-Lewis, R., Al-Darmarki, S., Flinko, R., Lovo, E., Wu, X., Robinson, J.E., Seaman, M.S., et al. (2013). Diverse specificity and effector function among human antibodies to HIV-1 envelope glycoprotein epitopes exposed by CD4 binding. Proc. Natl. Acad. Sci. USA *110*, E69–E78.

Günther, S., and Sundberg, E.J. (2014). Molecular determinants of agonist and antagonist signaling through the IL-36 receptor. J. Immunol. *193*, 921–930.

Guttman, M., Weis, D.D., Engen, J.R., and Lee, K.K. (2013). Analysis of overlapped and noisy hydrogen/deuterium exchange mass spectra. J. Am. Soc. Mass Spectrom. *24*, 1906–1912.

Hayakawa, H., Hayakawa, M., Kume, A., and Tominaga, S. (2007). Soluble ST2 blocks interleukin-33 signaling in allergic airway inflammation. J. Biol. Chem. *282*, 26369–26380.

Houde, D., Berkowitz, S.A., and Engen, J.R. (2011). The utility of hydrogen/deuterium exchange mass spectrometry in biopharmaceutical comparability studies. J. Pharm. Sci. *100*, 2071–2086.

Huang, J., Gao, X., Li, S., and Cao, Z. (1997). Recruitment of IRAK to the interleukin 1 receptor complex requires interleukin 1 receptor accessory protein. Proc. Natl. Acad. Sci. USA *94*, 12829–12832.

Ju, G., Labriola-Tompkins, E., Campen, C.A., Benjamin, W.R., Karas, J., Plocinski, J., Biondi, D., Kaffka, K.L., Kilian, P.L., Eisenberg, S.P., et al. (1991). Conversion of the interleukin 1 receptor antagonist into an agonist by site-specific mutagenesis. Proc. Natl. Acad. Sci. USA *88*, 2658–2662.

Junttila, I.S., Creusot, R.J., Moraga, I., Bates, D.L., Wong, M.T., Alonso, M.N., Suhoski, M.M., Lupardus, P., Meier-Schellersheim, M., Engleman, E.G., et al. (2012). Redirecting cell-type specific cytokine responses with engineered interleukin-4 superkines. Nat. Chem. Biol. *8*, 990–998.

Kabsch, W. (2010). Xds. Acta Crystallogr. D Biol. Crystallogr. *66*, 125–132.

Krissinel, E., and Henrick, K. (2007). Inference of macromolecular assemblies from crystalline state. J. Mol. Biol. *372*, 774–797.

Lefrançais, E., Roga, S., Gautier, V., Gonzalez-de-Peredo, A., Monsarrat, B., Girard, J.P., and Cayrol, C. (2012). IL-33 is processed into mature bioactive forms by neutrophil elastase and cathepsin G. Proc. Natl. Acad. Sci. USA *109*, 1673–1678.

Lefrançais, E., Duval, A., Mirey, E., Roga, S., Espinosa, E., Cayrol, C., and Girard, J.P. (2014). Central domain of IL-33 is cleaved by mast cell proteases for potent activation of group-2 innate lymphoid cells. Proc. Natl. Acad. Sci. USA *111*, 15502–15507.

Liew, F.Y., Girard, J.P., and Turnquist, H.R. (2016). Interleukin-33 in health and disease. Nat. Rev. Immunol. *16*, 676–689.

Lingel, A., Weiss, T.M., Niebuhr, M., Pan, B., Appleton, B.A., Wiesmann, C., Bazan, J.F., and Fairbrother, W.J. (2009). Structure of IL-33 and its interaction with the ST2 and IL-1RAcP receptors–insight into heterotrimeric IL-1 signaling complexes. Structure *17*, 1398–1410.

Liu, X., Hammel, M., He, Y., Tainer, J.A., Jeng, U.S., Zhang, L., Wang, S., and Wang, X. (2013). Structural insights into the interaction of IL-33 with its receptors. Proc. Natl. Acad. Sci. USA *110*, 14918–14923.

Lott, J.M., Sumpter, T.L., and Turnquist, H.R. (2015). New dog and new tricks: evolving roles for IL-33 in type 2 immunity. J. Leukoc. Biol. *97*, 1037–1048.

Luchini, A., Espina, V., and Liotta, L.A. (2014). Protein painting reveals solvent-excluded drug targets hidden within native protein-protein interfaces. Nat. Commun. *5*, 4413.

Lüthi, A.U., Cullen, S.P., McNeela, E.A., Duriez, P.J., Afonina, I.S., Sheridan, C., Brumatti, G., Taylor, R.C., Kersse, K., Vandenabeele, P., et al. (2009). Suppression of interleukin-33 bioactivity through proteolysis by apoptotic caspases. Immunity *31*, 84–98.

McCoy, A.J., Grosse-Kunstleve, R.W., Adams, P.D., Winn, M.D., Storoni, L.C., and Read, R.J. (2007). Phaser crystallographic software. J. Appl. Cryst. *40*, 658–674.

Mendoza, J.L., Schneider, W.M., Hoffmann, H.H., Vercauteren, K., Jude, K.M., Xiong, A., Moraga, I., Horton, T.M., Glenn, J.S., de Jong, Y.P., et al. (2017). The IFN-λ-IFN-λR1-IL-10Rβ Complex Reveals Structural Features Underlying Type III IFN Functional Plasticity. Immunity *46*, 379–392.

Molofsky, A.B., Savage, A.K., and Locksley, R.M. (2015). Interleukin-33 in Tissue Homeostasis, Injury, and Inflammation. Immunity *42*, 1005–1019.

Moraga, I., Richter, D., Wilmes, S., Winkelmann, H., Jude, K., Thomas, C., Suhoski, M.M., Engleman, E.G., Piehler, J., and Garcia, K.C. (2015). Instructive roles for cytokine-receptor binding parameters in determining signaling and functional potency. Sci. Signal. *8*, ra114.

Nagata, A., Takezako, N., Tamemoto, H., Ohto-Ozaki, H., Ohta, S., Tominaga, S., and Yanagisawa, K. (2012). Soluble ST2 protein inhibits LPS stimulation on monocyte-derived dendritic cells. Cell. Mol. Immunol. *9*, 399–409.

Nielsen, S.S., Toft, K.N., Snakenborg, D., Jeppesen, M.G., Jacobsen, J.K., Vestergaard, B., Kutter, J.P., and Arleth, L. (2009). BioXTAS RAW, a software program for high-throughput automated small-angle X-ray scattering data reduction and preliminary analysis. Journal of Applied Crystallography. *42*, 959–964.

Nold-Petry, C.A., Lo, C.Y., Rudloff, I., Elgass, K.D., Li, S., Gantier, M.P., Lotz-Havla, A.S., Gersting, S.W., Cho, S.X., Lao, J.C., et al. (2015). IL-37 requires the receptors IL-18Rα and IL-1R8 (SIGIRR) to carry out its multifaceted

anti-inflammatory program upon innate signal transduction. Nat. Immunol. *16*, 354–365.

Rider, P., Carmi, Y., Voronov, E., and Apte, R.N. (2013). Interleukin-1α. Semin. Immunol. *25*, 430–438.

Sattler, S., Smits, H.H., Xu, D., and Huang, F.P. (2013). The evolutionary role of the IL-33/ST2 system in host immune defence. Arch. Immunol. Ther. Exp. (Warsz.) *61*, 107–117.

Schmitz, J., Owyang, A., Oldham, E., Song, Y., Murphy, E., McClanahan, T.K., Zurawski, G., Moshrefi, M., Qin, J., Li, X., et al. (2005). IL-33, an interleukin-1-like cytokine that signals via the IL-1 receptor-related protein ST2 and induces T helper type 2-associated cytokines. Immunity *23*, 479–490.

Selzer, T., Albeck, S., and Schreiber, G. (2000). Rational design of faster associating and tighter binding protein complexes. Nat. Struct. Biol. *7*, 537–541.

Svergun, D. (1992). Determination of the regularization parameter in indirect-transform methods using perceptual criteria. Journal of Applied Crystallography. *25*, 495–503.

Takegawa, K., Yamabe, K., Fujita, K., Tabuchi, M., Mita, M., Izu, H., Watanabe, A., Asada, Y., Sano, M., Kondo, A., et al. (1997). Cloning, sequencing, and expression of Arthrobacter protophormiae endo-beta-N-acetylglucosaminidase in Escherichia coli. Arch. Biochem. Biophys. *338*, 22–28.

Takezako, N., Hayakawa, M., Hayakawa, H., Aoki, S., Yanagisawa, K., Endo, H., and Tominaga, S. (2006). ST2 suppresses IL-6 production via the inhibition of IkappaB degradation induced by the LPS signal in THP-1 cells. Biochem. Biophys. Res. Commun. *341*, 425–432.

Thomas, C., Moraga, I., Levin, D., Krutzik, P.O., Podoplelova, Y., Trejo, A., Lee, C., Yarden, G., Vleck, S.E., Glenn, J.S., et al. (2011). Structural linkage between ligand discrimination and receptor activation by type I interferons. Cell *146*, 621–632.

Thomas, C., Bazan, J.F., and Garcia, K.C. (2012). Structure of the activating IL-1 receptor signaling complex. Nat. Struct. Mol. Biol. *19*, 455–457.

Towne, J.E., Renshaw, B.R., Douangpanya, J., Lipsky, B.P., Shen, M., Gabel, C.A., and Sims, J.E. (2011). Interleukin-36 (IL-36) ligands require processing for full agonist (IL-36α, IL-36β, and IL-36γ) or antagonist (IL-36Ra) activity. J. Biol. Chem. *286*, 42594–42602.

Tsutsumi, N., Kimura, T., Arita, K., Ariyoshi, M., Ohnishi, H., Yamamoto, T., Zuo, X., Maenaka, K., Park, E.Y., Kondo, N., et al. (2014). The structural basis for receptor recognition of human interleukin-18. Nat. Commun. *5*, 5340.

Vigers, G.P., Anderson, L.J., Caffes, P., and Brandhuber, B.J. (1997). Crystal structure of the type-I interleukin-1 receptor complexed with interleukin-1beta. Nature *386*, 190–194.

Vyncke, L., Bovijn, C., Pauwels, E., Van Acker, T., Ruyssinck, E., Burg, E., Tavernier, J., and Peelman, F. (2016). Reconstructing the TIR Side of the Myddosome: a Paradigm for TIR-TIR Interactions. Structure *24*, 437–447.

Wang, X., Lupardus, P., Laporte, S.L., and Garcia, K.C. (2009). Structural biology of shared cytokine receptors. Annu. Rev. Immunol. *27*, 29–60.

Wang, D., Zhang, S., Li, L., Liu, X., Mei, K., and Wang, X. (2010). Structural insights into the assembly and activation of IL-1β with its receptors. Nat. Immunol. *11*, 905–911.

Weis, D.D., Wales, T.E., Engen, J.R., Hotchko, M., and Ten Eyck, L.F. (2006). Identification and characterization of EX1 kinetics in H/D exchange mass spectrometry by peak width analysis. J. Am. Soc. Mass Spectrom. *17*, 1498–1509.

Wilkins, M.R., Gasteiger, E., Bairoch, A., Sanchez, J.C., Williams, K.L., Appel, R.D., and Hochstrasser, D.F. (1999). Protein identification and analysis tools in the ExPASy server. Methods Mol. Biol. *112*, 531–552.

Yang, C.Y., Delproposto, J., Chinnaswamy, K., Brown, W.C., Wang, S., Stuckey, J.A., and Wang, X. (2016). Conformational Sampling and Binding Site Assessment of Suppression of Tumorigenicity 2 Ectodomain. PLoS ONE *11*, e0146522.

STAR★METHODS

KEY RESOURCES TABLE

REAGENT or RESOURCE	SOURCE	IDENTIFIER
Antibodies		
Monoclonal anti-gp120 N12-i3	Guan et al., 2013; in house	N/A
Bacterial and Virus Strains		
E. coli BL21(DE3) pLysS	Millipore Sigma	Cat#69451
Chemicals, Peptides, and Recombinant Proteins		
Naphthionic Acid	Sigma Aldrich	Cat#70862
Fast Blue B salt	Sigma Aldrich	Cat#D9805
Fast Red RC salt	Sigma Aldrich	Cat#44750
Fast Dark Blue R salt	Sigma Aldrich	Cat#F0750
Acid orange 50	Sigma Aldrich	Cat#S468576
Trypan blue	MP Biomedicals	Cat#02195532
Erythrosine B	TCI America	Cat#T0557
Deuterium Oxide (D2O)	Cambridge Isotope Laboratories	Cat#DLM-11-100
Kifunensine	GlycoFineChem	Cat#FC-034
TEV	In house	N/A
EndoA	In house	N/A
Carboxypeptidase A	Sigma Aldrich	Cat#C9268
Carboxypeptidase B	Sigma Aldrich	Cat#C9584
Critical Commercial Assays		
Nano-Glo Luciferase Assay	Promega	Cat#N1120
Nano-Glo Dual-Luciferase Reporter Assay	Promega	Cat#N1610
FugeneHD	Promega	Cat#E2311
Superdex75, prep grade	GE Healthcare	Cat#17104401
Superdex 200, prep grade	GE Healthcare	Cat#17104301
HisTrap excel	GE Healthcare	Cat#17-3712-05
HiTrap ConA	GE Healthcare	Cat#28-9520-85
HisPur NiNTA resin	ThermoFisher Scientific	Cat#88221
Deposited Data		
IL-33:ST2:IL-1RAcP structure	This study	PDB: 5VI4
Experimental Models: Cell Lines		
HEK293T	ATCC	Cat#CRL-3216
Recombinant DNA		
pET30	Millipore Sigma	Cat#69909
pcDNA4/TO	Thermo Fisher Scientific	Cat#V102020
pNL2.2	Promega	Cat#N1071
pGL4.53	Promega	Cat#E5011
Software and Algorithms		
Clustal Omega	Goujon et al., 2010	http://www.ebi.ac.uk/Tools/msa/clustalo/
Phenix	Adams et al., 2010	http://phenix-online.org/
Phaser (as part of Phenix)	McCoy et al., 2007	http://phenix-online.org/
Coot	Emsley et al., 2010	http://www2.mrc-lmb.cam.ac.uk/personal/pemsley/coot/
XDS	Kabsch, 2010	http://xds.mpimf-heidelberg.mpg.de/
Aimless (as part of CCP4)	Evans and Murshudov, 2013	http://www.ccp4.ac.uk/html/aimless.html
PISA (as part of CCP4)	Krissinel and Henrick, 2007	http://www.ebi.ac.uk/pdbe/pisa/

(*Continued on next page*)

Continued

REAGENT or RESOURCE	SOURCE	IDENTIFIER
BioXTASRaw	Nielsen et al., 2009	http://sourceforge.net/projects/bioxtasraw/
GNOM	Svergun, 1992	http://www.embl-hamburg.de/biosaxs/gnom.html
DAMMIF	Franke and Svergun, 2009	http://www.embl-hamburg.de/biosaxs/dammif.html
PLGS 2.5.1	Waters	http://www.waters.com
DynamX 3.0	Waters	http://www.waters.com
PyMol	Schrödinger	http://www.pymol.org/
Biacore T100 Evaluation Software	GE Healthcare	http://www.biacore.com
GraphPad Prism 5	GraphPad Software	http://www.graphpad.com/

CONTACT FOR REAGENT AND RESOURCE SHARING

Further information and requests for resources and reagents should be directed to and will be fulfilled by the Lead Contact, Eric J. Sundberg (esundberg@ihv.umaryland.edu).

EXPERIMENTAL MODEL AND SUBJECT DETAILS

For protein expression in *E. coli*, strain BL21(DE3)pLysS was used. Transformed cells were grown in shaker flasks in LB medium at 37°C until OD600 of 0.6, temperature was reduced to 18°C and protein expression induced by addition of 0.1 mM IPTG. Cells were harvested after 18 hr and kept frozen until protein purification.

For protein expression in HEK293T cells, cells were grown in shaker flasks in Freestyle F17 medium (Thermo Fisher Scientific), supplemented with GlutaMAX and Geneticin at 37°C and 5% CO2. For cell signaling assays, HEK293T cells were grown under the same conditions but in static culture. Cell line identity was not separately verified.

METHOD DETAILS

Plasmids and Proteins

The proteins and genes used correspond to the following UNIPROT database entries: murine IL-33 (ID Q8BVZ5), human IL-33 (O95760), human IL-1β (P01584, containing an additional serine at the amino-terminus), murine ST2 (P14719), human ST2 (Q01638), human IL-1RI (P14778), murine IL-1RAcP (Q61730), and human IL-1RAcP (Q9NPH3). For expression of cytokines, murine IL-33 (residues 108-266), human IL-33 (112-270) and human IL-1β (116-269, with mutation D116S) were subcloned into plasmid pET30 containing an N-terminal hexahistidine-tag followed by a TEV protease site. All receptor DNA was subcloned into pcDNA4/TO (ThermoFisher Scientific) replacing their native secretion signal with the one found in plasmid pHLsec (Aricescu et al., 2006), except for full length ST2 and human IL-1RAcP, which were cloned with their native secretion peptide. In particular, the following residues were subcloned: murine ST2 (26-326), human ST2 (19-321), human IL-1RI (18-336), murine IL-1RAcP (21-350), and human IL-1RAcP (1-350). After secretion peptide removal, human ST2 and murine IL-1RAcP contained three additional amino acids at their amino-termini (glutamine, threonine, and glycine). For binding studies, human IL-1RAcP was fused to human IgG_1-Fc. Except for full length ST2, all receptor proteins contained a hexahistidine-tag at their carboxy-terminus. All point mutations were generated following the Quikchange protocol (Agilent). Clustal Omega (Goujon et al., 2010) was used for sequence alignments.

Protein Expression and Purification

All cytokines were expressed in *E. coli*, typically overnight at 18°C. After cell lysis, proteins were purified by IMAC (HisPur NiNTA resin, ThermoFisher Scientific). The His-tag was removed by TEV digest and untagged cytokines were purified by another pass over a NiNTA column. All receptors were expressed transiently in HEK293T cells. After transfection using PEI, cells were cultured for 84 hr in Freestyle F17 medium, supplemented with GlutaMAX and Geneticin (Thermo Fisher Scientific). Proteins were purified from the supernatant using IMAC (His Trap Excel, GE Healthcare). As a final step all proteins were purified by size-exclusion chromatography (SEC) in 10 mM HEPES, pH 7.4, 150 mM NaCl (cytokines using Superdex75 and receptors and complexes using Superdex200, prep grade media, GE Healthcare). All cytokine preparations (except those used for crystallization) contained additionally 2 mM DTT.

Crystallization and Structure Determination

It has been suggested that activity of IL-33 is auto-regulated by oxidation of its cysteine residues (Cohen et al., 2015). Accordingly, for crystallization, all four cysteines in the mature cytokine were mutated to serine. The receptor proteins were deglycosylated. During transient expression, HEK cell cultures were supplemented with kifunensine (1 μg/mL) and resulting high-mannose type N-linked

glycosylation was removed using EndoA from *Arthrobacter protophormiae* (Takegawa et al., 1997) (produced in house). Initial attempts to deglycosylate the wild-type proteins revealed that the proteins were incompletely deglycosylated. Mass-spectrometric analysis revealed that some N-linked glycosylation sites were entirely refractory to enzymatic digest and that others were incompletely glycosylated. Thus, several N-linked glycosylation sites in mIL-1RAcP were mutated to glutamine (N107Q, N111Q, N196Q, N209Q) to generate mIL-1RAcP for crystallization. Removal of similarly identified partially and non-deglycosylated N-linked glycan sites in mST2 led to poor yields and therefore wild-type mST2 was used for crystallization. To increase homogeneity of deglycosylated proteins, mIL-33:ST2 and mIL-1RAcP were separately passed over a column with immobilized Concanavalin A (GE Healthcare). The flow through was then purified by SEC, proteins were concentrated, and mIL-33:ST2 and mIL-1RAcP were mixed at an equimolar ratio, incubated for 1 hr at RT and again passed over a size-exclusion column. The complex was concentrated to 7 to 8 mg/mL and subjected to crystallization by vapor-diffusion. Initially, clustered needles grew in the PEG/Ion Screen (Hampton Research) in 20% PEG 3350, 0.2M NaMalonate, pH 6. The crystal form was slightly improved by the addition of 0.2 M NaThiocyanate and repeated rounds of microseeding. Finally, in situ proteolysis with 1/100 (m/m) Carboxypeptidase A and Carboxypeptidase B (Sigma-Aldrich) further improved the crystal form. The final crystal grew in 16% PEG 3350, 0.2 M NaMalonate, pH 6, 0.2 M NaThiocyanate. Crystals were cryo-protected by soaking in mother liquor supplemented with 20% (v/v) glycerol. A dataset was collected from a single crystal at APS beamline GMCA 23-ID_D.

The dataset was processed using the XDS package (Kabsch, 2010) and AIMLESS (Evans and Murshudov, 2013). Initial phases were obtained by molecular replacement using the program PHASER (McCoy et al., 2007) using the model of murine IL-1RAcP (PDB: 4YFD) and human ST2:IL-33 (PDB: 4KC3) with all non-conserved side chains truncated to their Cβ-atom as a search model. The final model was built using iterative rounds of refinement with the Phenix program package (Adams et al., 2010) interspersed with manual model building in COOT (Emsley et al., 2010). The final model was deposited with the accession code PDB: 5VI4. Buried surface area was assessed through PISA (Krissinel and Henrick, 2007). Structure representations were generated with PyMol (The PyMOL Molecular Graphics System, Schrödinger, LLC).

Small Angle X-Ray Scattering (SAXS)

SAXS data were collected at Cornell High Energy Synchrotron Source, beamline G1, using a dual Pilatus 100K-S SAXS/WAXS detector (Acerbo et al., 2015). Each protein complex was measured at 5, 2.5 and 1.25 mg/mL in 10 mM HEPES, pH 7.4, 150 mM NaCl, 2% (v/v) glycerol. Protein concentration was determined by absorption at 280 nm with extinction coefficients calculated from the relevant protein sequences using ProtParam (Wilkins et al., 1999). Both for human and mouse IL-33 ternary complexes, IL-33 mutants with all of their cysteine replaced by serines were used. The samples exhibited no concentration-dependent effects within the sampled range, and for subsequent analysis the scattering profile of the highest concentration was used. Data were averaged from ten 1 s exposures of an oscillating sample. Initial data analysis was conducted using the BioXTAS RAW software (Nielsen et al., 2009). Radial distribution functions were calculated using GNOM (Svergun, 1992), and molecular envelopes were generated using DAMMIF (Franke and Svergun, 2009).

Direct Binding Analysis

Kinetic parameters and affinities of protein-protein interactions were measured by surface plasmon resonance (SPR) analysis using a Biacore T100 biosensor (GE Healthcare). 1000 response units (RU) of Protein A from Staphylococcus aureus (Sigma Aldrich) were immobilized on all channels of a CM5 sensor chip. Approximately 150 RU of Fc-tagged IL-1RAcP were directly captured from cell-culture supernatants on flow cell 2. On reference flow cell 1 the unrelated antibody N12-i3 (Guan et al., 2013) was captured at the same level (150 RU). Binding experiments were carried out in 10 mM HEPES, pH 7.4, 150 mM NaCl, 0.05% (v/v) Tween20 at 25C by single cycle kinetic analysis using five concentrations of a threefold titration series for ST2:IL-33 binding or a twofold titration series for IL-1RI:IL-1β binding, if not indicated otherwise. In between runs the sensor surface was regenerated with two 30 s injections of 20 mM HCl. Sensorgrams were double referenced against the control flow cell and buffer injections. Data were fit to a 1:1 binding model using the Biacore T100 Evaluation Software.

Signaling Studies

To measure the activities of cytokine variants, HEK293T cells were transiently transfected with a luciferase gene (nano-Luc, plasmid pNL2.2, Promega) under the control of the IL-8 promoter (Towne et al., 2011) using FugeneHD (Promega). For measurement of IL-1β and variants thereof, cells were only transfected with the reporter gene construct as the cells endogenously express IL-1RAcP and IL-1RI (Huang et al., 1997). For analysis of IL-33 and its variants, cells were additionally transfected with full length ST2 (with a mass ratio of reporter to receptor plasmid of 25/1). For analysis of ST2 mutants, cells were also transfected with a second, constitutively active reporter gene (pGL4.53, Promega) to allow for normalization of transfection efficiency. 18 hr after transfection, cells were harvested and seeded into 96 well plates at a concentration of 40,000 cells/well. Cells were stimulated with 5 pM IL-33 or 100 pM IL-1β. Initial titrations showed that both receptors are well below full activation at these concentrations. After 5 hr stimulation, cells were lysed and luciferase activity was determined using a Veritas luminescence reader (Promega).

Hydrogen-Deuterium-Exchange Mass Spectrometry

The coverage maps for all proteins were obtained from undeuterated controls as follows: 3 μL of ~50 μM sample in 10 mM HEPES, pH 7.4, 150 mM NaCl was diluted with 27 μL of the same buffer at room temperature followed by the addition of 30 μL of ice cold

quench (100 mM Glycine, 6.4 M Guanidine-HCl, 100mM TCEP, pH 2.4). After 2 min, 60 μL of 100mM Glycine buffer, pH 2.5 was added prior to the injection. The quenched samples were injected into a Waters HDX nanoAcquity UPLC (Waters; Milford, MA) with in-line pepsin digestion (Waters Enzymate BEH pepsin column). Peptic fragments were trapped on an Acquity UPLC BEH C18 peptide trap and separated on an Acquity UPLC BEH C18 column. A 7 min, 5% to 35% acetonitrile (0.1% formic acid) gradient was used to elute peptides directly into a Waters Synapt G2 mass spectrometer (Waters; Milford, MA). MSE data were acquired with a 20 to 30 V ramp trap CE for high energy acquisition of product ions as well as continuous lock mass (Leu-Enk) for mass accuracy correction. Peptides were identified using the ProteinLynx Global Server 2.5.1 (PLGS) from Waters. Further filtering of 0.3 fragments per residue was applied in DynamX 3.0.

For each construct, the HD exchange reactions were performed as follows: 3 μL of ~50 μM sample in 10 mM HEPES, pH 7.4, 150 mM NaCl was incubated in 27 μL of 10 mM HEPES, 99.99% D2O, pD 7.4, 150 mM NaCl. All ST2 complexes and controls (ternary, binary and IL-1RAcP) were acquired using a LEAP autosampler controlled with HDxDirector, whereas all IL-1RI complexes and control were acquired by manual quenching and injection. All reactions were performed at 25°C. Prior to injection, deuteration reactions were quenched at various times (10 s, 1 min, 10 min, 1 hr and 2 hr) with 30 μL of 100 mM Glycine buffer, 6.4 M Guanidine-HCl, 100 mM TCEP pH 2.4, followed 2 min later by the addition of 60 μL of 100mM Glycine buffer, pH 2.4. Back exchange correction was performed against fully deuterated controls acquired by incubating 3 μL of 50 μM of each sample in 27 μL 10 mM HEPES, 99.99% D2O, pD 7.4, 150 mM NaCl containing 7 M deuterated Guanidine DCl and 5 mM TCEP for 2 hr at 25°C prior to quenching (without guanidine HCl). All deuteration time points and controls were acquired in triplicate.

The deuterium uptake by the identified peptides through increasing deuteration time and for the fully deuterated control was determined using Water's DynamX 2.0 software. Correction for back exchange of deuterium with hydrogen after quenching and quantitation of differences in normalized deuterium levels were carried out as described in (Houde et al., 2011). EX1 type cooperative unfolding was analyzed using HX-Express2 (Guttman et al., 2013).

Protein-Painting by Mass Spectrometry

Samples were prepared and analyzed as outlined previously (Luchini et al., 2014). In particular, a mix of six different dyes (Figure S4A) was suspended at 5 mg/mL in 10 mM HEPES, pH 7.4, 150 mM NaCl. Dye 1, Dye 2 and Dye 3 were synthesized by mixing equimolar concentrations of Naphthionic Acid with Fast Blue B salt, Fast Red RC salt, and Fast Dark Blue R salt, respectively. The powder mixtures were then dissolved in MilliQ water. After allowing the reaction to proceed for 15 min at room temperature, the dye solutions were spun down (10 min, 16.1 rcf, 25 C) and the supernatants used in protein painting immediately. Proteins were added to the dye mix at a final concentration of 1.2 μM in a total volume of 50 μl. Solutions were allowed to incubate for 2 min at room temperature under rotation. The samples were then loaded on size-sieving Sephadex columns (mini Quick Spin Oligo Columns, Sephadex G25, Roche) and centrifuged at 1,000 g for 1 min at room temperature. The flow-through was collected, denatured with urea (final concentration 2 M), reduced in 10 mM dithiothreitol (15 min at 37°C), alkylated with 50 mM iodoacetamide (15 min, room temperature in the dark) and digested with trypsin (Promega) at 1:10 (w/w) protease/protein ratio for 2 hr at 37°C. Solutions were acidified with 6 μL of glacial acetic acid to stop the trypsin reaction. Tryptic peptides were purified by Pierce C18 columns (Thermo Fisher Scientific, 89870) following manufacturer's instructions, and analyzed by reversed-phase liquid chromatography nanospray tandem MS (LC-MS/MS) using an Orbitrap Fusion Tribrid Mass Spectrometer (Thermo Fisher Scientific). After sample injection by autosampler, the C18 column (0.2 × 50mm, Michrom Bioresources, Inc.) was washed for 2 min with mobile phase A (0.1% formic acid) and peptides were eluted using a linear gradient of 0% mobile phase B (0.1% formic acid, 80% acetonitrile) to 50% mobile phase B in 40 min at 500 nanoliter min-1, then to 100% mobile phase B for an additional 5 min. The Orbitrap Fusion Tribrid mass spectrometer (Thermo) was operated in a data-dependent mode in which each full MS scan was followed by five MS/MS scans where the five most abundant molecular ions were dynamically selected for collision-induced dissociation (CID) using a normalized collision energy of 35%. Tandem mass spectra were searched against a custom-made database containing the sequences of IL-1β, IL-1RI, IL-1RAcP, IL-33, and ST2 with Proteome Discoverer Software (Thermo Scientific) using tryptic cleavage constraints. High-confidence peptide identifications were obtained by applying the following filter criteria to the search results: Xcorr versus charge > = 1.9, 2.2, 3.5 for 1+, 2+, 3+ ions; $\Delta Cn > 0.1$; probability of randomized identification ≤ 0.01. Comparison of differentially identified spectra allowed localization of interface residues (Figure S4B).

QUANTIFICATION AND STATISTICAL ANALYSIS

Details about the statistical analysis and sample size of the different experiments can be found in the figure legends. In general, we used single protein samples for the crystal structure determination, the small angle scattering studies, and the mass-spectrometry-based analysis, while the direct binding analysis and signaling studies were conducted with multiple biological replicates. Furthermore, at least three independent experiments were conducted in all cases except the X-ray-based studies. For HDX experiments data were given as mean ± SD while for SPR and signaling studies mean ± SEM was plotted. GraphPad Prism 5 was used for data plotting.

DATA AND SOFTWARE AVAILABILITY

The accession number for the crystal structure of IL-33:ST2:IL-1RAcP reported in this paper is PDB: 5VI4.